

Artificial Neonatal Airway Model

By

Jibril Mussa

A thesis submitted to



Auckland University of Technology
in fulfilment of the requirements of the degree of
Master of Philosophy

February 2012
School of Engineering

Primary Supervisor: Professor Ahmed Al-Jumaily

TABLE OF CONTENTS

TABLE OF CONTENTS.....	I
LIST OF FIGURES.....	V
LIST OF TABLES.....	VII
ATTESTATION OF AUTHORSHIP.....	VIII
ACKNOWLEDGEMENT.....	IX
ABSTRACT.....	X
CHAPTER 1: INTRODUCTION.....	1
1.1 BACKGRAOUND.....	1
1.2 LITERATURE REVIEW.....	2
1.3 OBJECTIVES.....	5
CHAPTER 2: AIRWAY CASTING.....	6
2.1 INTRODUCTION.....	6
2.2 AIRWAY CASTING.....	6
2.3 CORE MATERILAS USED FOR NEGATIVE CASTING.....	7
2.4 NEGATIVE CASTING.....	8
2.5 CORE MATERIALS FOR POSITIVE CASTING.....	10
2.6 POSITIVE CASTING.....	10
2.7 METHODOLOGY.....	11
2.7.1FIRST NEGATIVE CAST.....	11

2.7.2 MOLD MANUFACTURING.....	12
2.7.3 SECOND NEGATIVE CAST.....	14
2.7.4 POSITIVE (HOLLOW) CAST.....	15
2.8 CLOSURE.....	19
CHAPTER3: EXPERIMENTAL INVETIGATION.....	20
3.1 INTRODUCTION.....	20
3.2 LUNG SIMULATOR.....	20
3.2.1 PERSONAL COMPUTER.....	21
3.2.3 NATIONAL INSTRUMENTS EXTENDER BOARD.....	22
3.2.4 FUJI SERVO SYSTEM.....	23
3.2.5 SERVO MOTOR.....	24
3.2.6 PENUMATIC CYLINDER.....	25
3.2.7 DISPLACEMENT ENCODER.....	25
3.2.8 SAFETY MECHANISM.....	26
3.2.8.1 SAFETY SWITCHES.....	27
3.2.8.2 RELAY.....	27
3.3 AIRWAY TREE SETUP.....	27
3.4 PRESSURE MEASUREMENTS.....	28
3.5 FLOW METER.....	30
3.6 SHAKER.....	30

3.7 EXPERIMENTAL PROCEDURE.....	31
3.8 CLOSURE.....	33
CHAPTER 4: MODELLING.....	34
4.1 INTRODUCTION.....	34
4.2 MODELLING SYSTEM.....	34
4.3 MODELLING ASSUMPTION.....	35
4.4 MODEL DEVELOPMENT.....	36
4.5 SIMULINK MODEL.....	38
4.6 CLOSURE.....	40
CHAPTER 5: RESULTS.....	41
5.1 INTRODUCTION.....	41
5.2 AIRWAY TESTS ON 142 DAY LUNG CAST.....	41
5.2.1 BRONCHI #4 AND #19.....	41
5.2.2 BRONCHI #6 AND #21.....	42
5.2.3 BRONCHI #9 AND #23.....	42
5.2.4 BRONCHI #13 AND #28.....	42
5.3 AIRWAY TESTS ON 128 DAY LUNG CAST.....	47
5.3.1 BRONCHI #3 AND #16.....	47
5.3.2 BRONCHI #12 AND #27.....	47
5.3.3 BRONCHI #4 AND #25.....	47

5.3.4 BRONCHI #14 AND #23.....	47
5.4 MODELLING RESULT.....	52
CHAPTER 6: DISCUSSION.....	54
6.1 INTRODUCTION.....	54
6.2 ENHANCED CASTING PROCESS.....	54
6.3 EXPERIMENTAL RESULT.....	55
6.4 STATISTICAL ANALYSIS.....	57
6.5 MODELLING RESULT.....	60
CHAPTER 7: CONCLUSION AND FUTURE WORK.....	63
7.1 CONCLUSION	63
7.2 FUTURE WORK.....	63
REFERENCE.....	65
APPENDICES.....	68
APPENDIX A: MATLAB PROGRAM.....	68
APPINDIX B: FLOW CHART.....	69

LIST OF FIGURES

Figure 2.1a: Silicon injected lung.....	12
Figure 2.1b: After maceration by KOH.....	12
Figure 2.2: Mold manufacturing process.....	14
Figure 2.3: Second negative embedded into the mold.....	15
Figure 2.4 Painted Wax samples.....	16
Figure 2.5: Painted negative cast.....	17
Figure 2.6: Final hollow airway cast.....	17
Figure 2.7: Schematic diagram for 142 day gestation lamb cast.....	18
Figure 2.8: Schematic diagram for 128 day gestation lamb cast.....	19
Figure 3.1: Lung simulator setup.....	21
Figure 3.2: Labview Block diagram.....	22
Figure 3.3: National Instruments Extender board.....	23
Figure 3.4: Servo Amplifier.....	24
Figure 3.5: Servo Motor.....	24
Figure 3.6: Pneumatic Cylinder.....	25
Figure 3.7: Displacement Encoder.....	26
Figure 3.8: Safety switches.....	26
Figure 3.9: Relay.....	27
Figure 3.10: Casted airway suspended in the Chamber.....	28
Figure 3.11: Pressure Transducer.....	30
Figure 3.12: Flow meter.....	30
Figure 3.13: Shaker with Cone.....	31
Figure 4.1: The Elements of the Ovine respiratory system model.....	35
Figure 4.2: Airways Subsystem.....	39
Figure 4.2: Overall Simulink model.....	40
Figure 5.1: Frequency spectrum of Lower Trachea (LT), Bronchioles (BR) #4 and (BR) #19 against Trachea (T).....	43
Figure 5.2: Frequency spectrum of Lower Trachea (LT), Bronchioles (BR) #6 and (BR) #21 against Trachea (T).....	44
Figure 5.3: Frequency spectrum of Lower Trachea (LT), Bronchioles (BR) #9 and (BR) #23 against Trachea (T).....	45

Figure 5.4: Frequency spectrum of Lower Trachea (LT), Bronchioles (BR) #13 and (BR) #28 against Trachea (T).....	46
Figure 5.5: Frequency spectrum of Lower Trachea (LT), Bronchioles (BR) #3 and (BR) #16 against Trachea (T).....	48
Figure 5.6: Frequency spectrum of Lower Trachea (LT), Bronchioles (BR) #12 and (BR) #27 against Trachea (T).....	49
Figure 5.7: Frequency spectrum of Lower Trachea (LT), Bronchioles (BR) #4 and (BR) #25 against Trachea (T).....	50
Figure 5.8: Frequency spectrum of Lower Trachea (LT), Bronchioles (BR) #14 and (BR) #23 against Trachea (T).....	51
Figure 5.9: Frequency spectrum of Airways at 0.5b/sec respiratory rate.....	52
Figure 5.10: Frequency spectrum of Airways at 0.5b/sec respiratory rate.....	53
Figure 5.11: Frequency spectrum of Airways at 0.5b/sec respiratory rate.....	53
Figure 6.1: Highest amplitude of each Bronchiole at particular breathing rate, from 142 g lamb cast.....	55
Figure 6.2: Highest amplitude of each Bronchiole at particular breathing rate, from 128 g lamb cast.....	55
Figure 6.3: Frequencies with the highest amplitude at each bronchiole, from 142 g lamb cast.....	56
Figure 6.4: Frequencies with the highest amplitude at each bronchiole, from 128 g lamb cast.....	56
Figure 6.5 Statistical graphs from 142d gestation lamb experimental result using different respiratory rate values.....	58
Figure 6.6 Statistical graphs from 128d gestation lamb experimental result using different respiratory rate values.....	59
Figure 6.7: Frequencies with the highest amplitude at each airway.....	60
Figure 6.8: Highest amplitude for each airway at particular breathing rate.....	61
Figure 6.9: Model Vs Experimental pressure value comparison.....	62

LIST OF TABLES

Table 2.1: Materials used for positive (hollow) casting.....	13
Table 2.2: Airway generation and their thickness.....	16
Table 3.1: Wire and Pin configuration on National Instruments Extender board.....	23
Table 3.2: List of pressure sensors.....	29
Table 3.3: Experimental Parameters for each branch.....	33
Table 6.1a: Model Vs Experimental pressure value comparison.....	62
Table 6.1b: Model Vs Experimental pressure value comparison.....	62

ATTESTATION OF AUTHORSHIP

I hereby declare that this submission is my own work and that, to the best of my knowledge and belief, it contains no material previously published or written by another person (except where explicitly defined in the acknowledgements), nor material which to a substantial extent has been submitted for the award of any other degree or diploma of a university or other institution of higher learning.

Jibril Mussa

February 2012

ACKNOWLEDGEMENTS

I will forever remain deeply thankful to my first supervisor, Professor Ahmed Al-Jumaily for his helpful suggestions, guidance and unwavering encouragement. His patience and support helped me to overcome many obstacles in the way of completing this thesis.

I express a sincere gratitude to my second supervisor Dr. Geoff Bold from Fisher and Paykel healthcare who made his valuable advice and support available to me throughout my work. I am grateful to Martin Leckie and Adam Darby from Fisher and Paykel Health care for accepting and supporting my project.

I owe my deepest gratitude to Technology for Industry Fellowships (TIF) who helped me to expose to industrial environment and improve technical skills by funding my project (FAPX0902).

My heartfelt thanks go to my fellow researchers in IBTec for their kindness and support throughout my study time.

A special thanks goes to Mohammed H.M. who made my study life extremely easy by providing a laptop which was instrumental for data collection and storage throughout this project. I thank the rest of my family for their ongoing support throughout my study.

I wish to express my love and gratefulness to my beloved mother for her prayer and encouragement to focus on my work throughout my study.

Finally, I would like to give special thanks to my wife Zahara who supported me mentally and helped me to concentrate on my study. Without her help and encouragement, this study would not have been completed.

ABSTRACT

The main aim of this project is to establish the effectiveness of Bubble CPAP in transmitting pressure oscillations through the neonatal tracheobronchial tree. As it is very difficult to establish how much of the pressure oscillation delivered to the mouth can reach the various branches during in-vivo measurements, this research focuses in developing an in-vitro experiment on the lung model.

Hollow lung models for 128 and 142 day gestation lambs were created from existing silicon lung casts. An experimental setup using a lung simulator and pressure sensors was developed. Different combinations of respiratory rate and frequencies with different amplitudes were used to perform experimental tests. The current ovine respiratory system which was available at IBTec was modified to reflect the current experimental setup. Computer simulations were performed and compared with the experimental results.

The study indicates that pressure waves with different frequencies can be delivered to different locations of the lung by controlling the pressure oscillation source to the lung.

CHAPTER 1

INTRODUCTION

1.1 Background

There are increasing numbers of low birth-weight and premature infants surviving with conditions such as chronic lung disease or bronchopulmonary dysplasia (BPD) due to complications of assisted mechanical ventilation and other factors. It is believed that the primary cause of respiratory distress syndrome (RDS) in premature infant is inadequate pulmonary surfactant [1]. Under normal circumstances, the lungs develop fully at 38 weeks of gestation allowing free gas exchange. However, when the babies are born at 26-27 weeks of gestation, inadequate small levels of surfactant will be secreted in the lung which prevents the alveoli from collapsing [1]. Even though the levels of surfactant are inadequate, the mechanism of gas exchange could still take place if the infant was born at this stage. However, it will be hard for the infant to keep the alveoli inflated between breaths which known to be RDS. Thus, it becomes appropriate to treat such premature infant with positive pressure respirators to keep the alveoli open by forcing the air into the alveoli.

A mechanical ventilator has been the traditional method of respiratory ventilation. Unfortunately, utilizing this type of ventilator on premature lungs is believed to cause RDS to develop into BPD. BPD occurs in premature infants usually born less than 30 weeks of gestation or 1200g at birth, resulting from lack of oxygen and mechanical ventilation [2].

Over the years various respiratory support devices have been introduced to help minimize the risk of over distention of the airways. The Bubble Continuous Positive Airway Pressure (CPAP) System introduced by Fisher and Paykel Healthcare Ltd was amongst the respiratory support devices developed. Bubble CPAP is a combined effect of CPAP and pressure oscillations from the bubbles. It provides an effective respiratory support to neonates with breathing difficulty. This system has been reported to have clinical benefits [2-5] compared to that of mechanical ventilation. Understanding of which frequency and how far those pressure oscillations can reach into various parts of the neonatal lung will help to improve the performance of the Bubble CPAP, hence this thesis undertaken.

1.2 Literature review

Early modes of mechanical ventilation include intermittent mandatory ventilation (IMV) and synchronized intermittent mandatory ventilation (SIMV) with pressure and volume control modes. These ventilators are used to maintain gas exchange in the respiratory system. IMV allows the delivery of a mechanical breathing cycle, at fixed pressure which often leads to asynchrony depending on the spontaneous breath of IMV [6]. Although this type of mechanical ventilation is often used as a life saving ventilation technique, it is believed to cause varying degrees of lung injury, especially with infants suffering with BPD, as a result of asynchrony between the patient breathing and IMV [6].

Synchronized mechanical ventilation was developed to allow mechanical breaths to be set synchronized with spontaneous inspiration through the use of signals that derived from spontaneous respiratory action. This technique with pressure support of each spontaneous breath is an approach which physiological decreases the work of breath imposed by the endotracheal tube and has been shown to avoid most of the problems associated with asynchronous ventilation[7].

Due to the high risk associated with the mechanical ventilation, continuous research has been undertaken in developing improved ventilation technology to minimize the complication of lung injury. These include high frequency ventilation (HFV), continuous positive airway pressure (CPAP) and biologically variable ventilation (BVV).

BVV is a computer based control mimicking the normal variability in spontaneous breathing to maintain gas exchange [8]. BVV allows better gas exchange and respiratory mechanics in porcine models of acute respiratory distress syndrome (ARDS), both in the presence and absence of end-expiratory pressure [9]. Mathematical modeling [9] and experiments in pigs with ARDS [8] shows that BVV improves gas exchange at similar mean airway pressures and minute ventilation compared with conventional ventilation. It is postulated that improvement in gas exchange occurs due to variations in end-inspiratory pressure from the variable tidal volumes [8]. This pressure variation increases recruitment of atelectatic regions seen in ARDS. Many studies have shown that stochastic resonance, as occurs in noisy ventilation techniques such as BVV and Bubble CPAP is responsible for alveolar recruitment, especially in atelectatic lungs [8].

The basis of HFV is to give sufficient ventilation of the lungs at high frequencies with tidal volumes equal to or less than the dead space, while keeping the mean airway pressure to a minimum [10]. HFV is a useful technique that can be used in patients of all ages who cannot breathe independently. It is especially useful in neonates with premature lungs. HFV is effective in keeping the lungs open, thus reducing the amount of inflation and deflation of the lungs. This coupled with its effect of lowering pressure variation decreases the risk of barotrauma to lung tissues. HFV is useful especially in the case of restrictive lung diseases such as emphysema and cystic adenomatoid malformation [10]. Previous clinical trials have shown that infants treated with HFV did not require supplemental oxygen at 36 weeks compared to those treated with conventional ventilation. In addition, there is a significant decrease in the number of days before extubation and an increase in the number of infants who survived without chronic lung disease [11, 12]. Bulk convection and molecular diffusion are the two common mechanisms of gas transport during normal breathing. In addition to these, it has been suggested that direct alveolar ventilation, pendelluft, convective gas transport, facilitated diffusion, and molecular diffusion contribute to gas transport in HFV.

Compared to endotracheal ventilation, Nasal Continuous Positive Airway Pressure (nCPAP) is a non-invasive type of respiratory support. A continuous positive pressure is delivered to the alveoli through nasal prongs or tubes during the respiratory cycle. The positive pressure is generated by variable resistance at exhalation. This allows a more regular breathing pattern compared to conventional ventilation. For this reason, nCPAP is becoming a popular choice in hospitals for the treatment of neonates with RDS [13, 14]. The positive pressure applied to the lungs is created by a variable resistance during exhalation. Because it allows the infant to breath spontaneously, nCPAP facilitates a more regular breathing pattern compared to mechanical ventilation. It uses jet flow at high velocity, which can entrain gas to assist inspiration on demand and keep the CPAP level constant[15]. This reduces the need for mechanical ventilation and oxygen delivery to the alveoli in infants with RDS with no harmful side effects[15].

Instead of variable resistors, the Bubble CPAP system consisted of an under-water seal to produce end-expiratory pressure. Infants receiving CPAP by under-water seal experienced vibration of their chest due to bubbling in the underwater seal caused by gas flow which was transmitted to the infant's airway. This maintains a degree of lung inflation during

expiration, thus preventing lung collapse and making it easier for the neonate to breathe. The vibrations simulated the waveforms produced by HFV when recorded on a pressure transducer attached to the infant's airway [16]. Bubble CPAP can decrease minute volume and respiratory rate without affecting alveolar ventilation. It can also contribute to gas exchange by causing chest vibrations, hence decreasing the infant's required work of breathing to maintain the same level of gas exchange [16].

Bubble CPAP has been used for the treatment of respiratory distress syndrome in newborn infants for over 30 years. It has attracted attention over the past 20 years because of the low incidence of chronic lung disease in preterm infants treated with Bubble CPAP [9]. Various studies have identified the benefit of using Bubble CPAP in managing RDS in neonates. B-CPAP can improve CO₂ clearance, improves arterial oxygen levels, minimise the chance of lung injury by decreasing the number of days required for mechanical ventilation and, improve gas exchange due to improved airway patency and lung volume requirement [9].

A previous study [17] clearly outlines the advantage of Bubble CPAP over the conventional (mechanical) treatment. A significant benefit of Bubble CPAP is increasing Functional Residual Capacity (FRC) by increasing transpulmonary pressure contributing to improved gas exchange. FRC is defined as the amount of air left in the lungs at the end of expiration. FRC is generally reduced in many lung diseases and when it falls below closing volume, airway closure may occur. Therefore, Bubble CPAP helps maintain the lung volume by avoiding alveolar collapse, and to allow alveolar gaseous exchange. Bubble CPAP involves lower chance of BPD development in preterm infant. This may be due to the avoidance of aggressive initiation of gas exchange with high tidal volumes and inadvertent hyperventilation that occurs in intubated infants. Bubble CPAP also protects the infant from standard mechanical ventilation and inadvertent over or under ventilation as well as airway injury and colonization from the endotracheal tube. Preterm lambs treated with Bubble CPAP [11] had fewer neutrophils, less hydrogen peroxide, and larger lung gas volumes than did the mechanically ventilated lambs. This is because Bubble CPAP improves the compliance of the lung by preventing repetitive inflammatory stresses on the preterm lung and preserves surfactant function better than mechanical ventilation. In addition, it has been suggested [18] that the noisy pressure signal promotes surfactant secretion in the lung.

A clinical study done by Pillow et al.[3] showed that adding pressure oscillations to CPAP ventilation will increase the compliance and decrease the airway resistance these in turn will improve a gas exchange.

Fredberg [19] and his team on their Simulations and experimental work done on normal adult lungs and on canine lungs respectively show that the geometry and mechanical properties of the lung are important factors in the mechanical response of the lung. They suggested that the elastic condition of the lung walls improve by the vibration caused by pressure oscillations. Study done on canine trachea[20] showed that increase in vibration frequency (up to 37Hz) will decrease in muscle stiffness.

In summary, mechanical ventilation is associated with significant lung tissue injury. This led to the development of various respiratory ventilators. Clinical and analytical studies have shown the benefit of adding pressure oscillations to CPAP ventilators. However which frequency and how far those pressure oscillations can reach into various parts of the neonatal lung are still unknown. This is the main motivation behind this research.

1.3 Objectives

The main aim of this project is to establish the effectiveness of Bubble CPAP in transmitting pressure oscillations through the neonatal tracheobronchial tree. As it is very difficult to establish how much of the pressure oscillation delivered to nasal cavity can reach the various branches, this research focuses on developing experiments on an artificial lung models. To achieve this, the objectives of the project are to:

- Build artificial airway models which include developing an appropriate procedure for lung casting.
- Develop an experimental setup and procedure to assess pressure oscillation transmission to various parts of the lung.
- Adapt the present computational model of the Ovine Neonatal Respiratory System which was developed by IBTec to represent the current artificial neonatal tracheobronchial tree used in the experiments.
- Determine the attenuation of different pressure oscillation frequencies and amplitudes along the tracheobronchial tree using the model.
- Compare the experimental and the modelling results.

CHAPTER 2

AIRWAY CASTING

2.1 Introduction

Since human neonatal lungs are not available, casting of ovine lungs is done as the closest approximation. Section 2.2 begins by introducing the types of casting and pre-existing casting processes. Types of materials used for negative casting and the process of making negative casts are given in sections 2.3 and 2.4 respectively. Section 2.5 and 2.6 discuss the materials and the processing respectively used for positive casting.

2.2 Airway Casting

Casting is a process involving molten materials (such as metals, plastics or resins) being poured into a mold, allowed to solidify and then extracted for use. It is a method for reproducing an element – whether a small part or a single unit by itself. Casting can be used to produce complex parts that would otherwise be too expensive or time-consuming to make using other methods such as cutting or shaping from solid.

Airway casts may be classified into two main components: negative casts, which are solid and they represent the lumen of the tube; and positive casts, which are hollow and represent the walls of the tube. Negative casts are used to demonstrate the anatomy of the bronchial tree, to measure the dimensions of the airways and their branching angles, count their numbers as well as to study the pattern of branching. Positive casts are used for experimental purposes involving fluid flow characteristics[21].

There are several types of materials that can be used to make casts. Different materials have different physical properties and the choice of material depends on the requirements of the technique being used. Cast making involves removing the tissues once the cast has been made using corrosive chemicals; hence it is important that the material from which the cast is made can withstand the chemicals (acid or alkali).

Negative casting requires strong and rigid or flexible materials that can withstand handling, pruning and measuring. Other important properties of a mold include; adjustable viscosity, constant volume on setting, immiscible with water and it should not penetrate the tissue.

In positive casting, a negative cast is first made to be used as mold for the positive cast and painted with another material. The negative cast is then removed usually by melting; hence a material of low melting is necessary for positive casting.

2.3 Core Materials used for Negative Casting

This section summarizes the materials used for negative casting.

Metallic alloys can be made with low melting points and used for lung casting. Woods metal with melting point of 70°C is most commonly used in casting. It is poured into a dry and fixed lung to avoid deformation due to its weight and problems that might arise from water-molten metal interface. It can be used to construct casts that can reach the alveoli, but careful control over the temperature is important to prevent the formation of a heavy cast that is hard to trim. Woods metals are no longer favorable in the making of final negative casts. However, it is still used to make the negative cast mold for positive casting [22].

Wax has been used previously to make negative casts [23-25]. There are many types of waxes available with a wide range of melting points which can be used for making lung casts. In some cases, dental waxes have been used; however paraffin wax (with melting point of 60°C) is sufficient. The processes of making negative wax casts is same as making metal casts and are similarly used to make positive casts. Wax casts are lighter and easier to remove but more fragile compared to metal casts.

Methyl Methacrylate was first introduced by Schummer in 1935 [26] for casting purposes. It can be used to construct fine structures such as capillaries however, polyester resins are preferred in bronchial tree casting [22].

Vinylite was first used to demonstrate pulmonary pathology by Liebow *et al.* 1947 [27] and was later improved for making vascular and bronchial casts. Vinylite dissolves in acetone and shrinks significantly upon solvent evaporation. It is also brittle and breaks easily hence, polyester resins are more preferred.

There are many different types of resins available with different physical properties that can be used for casting. Hence prior experiment is required to find the ideal properties for a given application. Polyester casts are strong and stable, but they are brittle when used to

make thin branch casts. The resins can be self colored for identification when making combined vascular and airway casts or can be painted to identify orders. [28, 29] Used resin for making negative casts.

There is a wide variety of Silicone rubbers used for casting purposes. Therefore prior experiment is required to find the one with the desired quality. Their ideal properties include stretchability, flexibility, and stable volume on setting, easily pruned by cutting and are immiscible with water. Phalen, Raabeet and Schreider [30-32] used Silicone for making negative casts. The main advantage of the silicon is that, it can be used in a wet condition which means there is no need for a dried lung; which saves a substantial amount of time.

2.4 Negative Casting

Negative casting is a process of making a solid element by pouring a liquid material into a mould which contains a hollow cavity of the desired element.

Frank and Yoder [33] made a flexible cast of the lung using Silastic RTV, a silicone rubber that vulcanizes at room temperature with the addition of a catalyst. Silastic has a short half life, hence Silastic no. 382 was chosen. The Silastic base silicone fluid and a catalyst stannous octoate were mixed thoroughly to ensure a uniform viscosity. The amount of catalyst added influences the viscosity and this in turn influences how far down into the lung the mixture will reach. The catalyst determines the working time of the mixture. The working time is the amount of time it takes for a thin skin to form over the exposed surface, hence bringing the flow of the mixture to a stop. Temperature and humidity also influence the process. The working time was typically 15 – 30 minutes and complete vulcanization took two or three days. The last step involved dissolving the tissue mold using Hydrochloric acid, to which Silastic is impermeable. The lungs were either dried with air or fixed with formaldehyde fumes (about 10%) at approximately constant pressure for 3 -4 days. Silicon is one of the best materials for making negative casts but it is hard to remove it if it is intended to make positive casts.

Viggiano et al. [34] presented a new simple injection technique based on expanded polyurethane, which allows preparing vascular and bronchial trees for a macroscopic and microscopic studies. Polyurethanes are a class of polymers produced by two components:

poly (ethylene glycol) and diisocyanate. By mixing these two components, the mixture expands and the result is stiff expanded polyurethane, which fills the cavities of vessels, reproducing their shape. The mixture is a closed-cell foam with a compact surface that reproduces with high definition the surface of the cavity filled by the foam. The polymer has a high resistance to bumps and compression, dimensional stability and a low index of water absorption. Moreover, it is resistant to concentrated NaOH, thus allowing the maceration of the tissue. The foam in free expansion increases its volume by 43%. However, the foams obtained in a closed volume (such as after injection in vessels) are much more compact than those obtained in free expansion. The liquid mixture is expelled by propelled air. A cannula 0.4 cm in diameter was inserted into the main conduit of the isolated organ. A forceps was used to maintain the cannula inside the main vessel of the organ, to achieve a uniform injection pressure. The cannula was then connected to the compressed air device containing polyurethane. This was injected until small vessels on the organ surface were visible. During injection the polyurethane cylinder was maintained vertically up-side-down to obtain uniform propulsion of the polyurethane. At the end of the injection the cannula was left for 5 min *in situ*, to allow complete polymerization. Moreover, the organ was left undisturbed for further 20min, to avoid any distortion of the vessels. The organ was then immersed in 10% NaOH at room temperature, renewing the liquid every day. After complete maceration the cast was air-dried.

Perry et al [35] used negative pressure casting techniques for obtaining silicone rubber casts of the avian respiratory system. The fresh left lung was inflated through the vasculature and airways with glutaraldehyde fixative (2.5% in 0.1 M phosphate buffer, pH 7.3) at pressures ranging from 20 to 30 cm of water. Following complete fixation, the upper and lower lobes were separated and their volumes measured by displacement. The segment was cannulated and repeatedly flushed with degassed saline. Cut airways through which casting material might escape during injection were located and tied off. For injection of a segmental bronchus, 50–100 mL of silicone elastomer was required. Three types of self-polymerizing silicone elastomers were tested and the elastomers were made less viscous by addition of three types of silicone oil (polydimethylsiloxan) at 10, 15, 20, 25, 30, 25 and 40 volume percent. Injection techniques using either positive and negative pressure or negative pressure alone were tested.

2.5 Core Materials used for Positive Casting

As mentioned previously, materials for positive casts need to be stable and strong to withstand the trauma that will result from the removal of the negative cast.

Pederson [36] used copper to electroplate a Woods metal negative cast to produce a hollow cast. The Woods metal was removed by melting to produce the positive cast. However, a silver coating is quicker and more evenly distributed [22].

Most synthetic latex is made from two materials; styrene and butadiene [37]. Both are currently obtained from petroleum. Synthetic latex is used in coating and glues because it solidifies by coalescence of the polymer particles as the water evaporates. Eisman [38] first coated a metal alloy negative cast with two layers of latex. The metal is removed by melting and squeezing using fine forceps.

Silicone rubbers are widely used in industry and there are multiple formulations. They are often one or two part polymers and contain fillers to improve properties or to reduce cost. They are generally not reactive, stable and resistant to extreme environment and temperature (-55 to +300 ° C) while still maintaining its useful properties. Due to these properties and its ease of manufacturing and shaping, silicone rubbers are found in a wide variety of products, including medical devices [39]. Silicone rubber was used to coat a wax negative cast by repeatedly painting it on and curing each coat. The wax is removed by heating, squeezing and blowing.

2.6 Positive Casting

Pedersen et al. [36] produced rigid hollow casts of the central airways of a dog using a Wood's metal negative electroplated directly with copper. The airways were dried with compressed air and left to dry for 72 hours. Then the Wood's metal with a melting point of 70°C was poured into the airways. To decrease the flow of the casting material into the airways, Pedersen cooled the lung first by putting the lung in a plastic bag and fully enveloping the lung with crushed ice. Once the metal solidified, the tissue was removed by sodium hydroxide in a period of 24-48hours. The Wood's metal was then removed by boiling water, steam and a propane torch.

Snyder et. al. [40] made a hollow cast of canine airways using a eutectic alloy and Plexiglas. The lung was cleaned and inflated to 25 cmH₂O to dry within 5 days. After the lung dried, a low-melting-point eutectic alloy was poured into the lung through the tracheal cannula. Then the tissue macerated using 5-M NaOH. Consecutive thirty coatings of Plexiglas were applied over the entire cast. The cast was then left in an oven set at 100°C for several hours in order to melt the eutectic alloy.

Schlesinger [41] used a silicon rubber coating on a negative wax to prepare a hollow airway cast. The lung was first cleaned and dried with a continuous air pressure. The drying process took around 7 days. Wax was heated to 72°C and poured through the trachea into the dried lung. The wax was left for 24 hours to dry. Then the tissue macerated by placing the lungs in NaOH and washed with a jet of water to remove loose tissue. The casted wax was repeatedly painted with silicone. Once the silicone cured, the wax was removed by heating, squeezing and blowing.

Unfortunately these trials have the disadvantage of being fragile, brittle, quick to shrink, relatively heavy or require air-dried lung. Also there is difficulty in removing the negative cast in order to achieve the hollow casting process. In this work, a novel technique based on producing a negative component from the lung is developed as follows.

2.7 Methodology

The following methodology was performed for manufacturing positive casts. Section 2.7.1 starts by describing the process of making the first negative cast, which was available at IBTec. Section 2.7.2 discusses the mold manufacturing method. Section 2.7.3 discusses making the second negative cast and section 2.7.4 mentions the process of positive casting.

2.7.1 First Negative Cast

The first negative was obtained from an earlier study performed by Reddy [42]. A brief summary of the methods used is given as follows.

- A 4.5 mm internal diameter endotracheal tube was inserted into the trachea. Two ties were used to fasten the tube to avoid slippage.
- A syringe was used to suck out any excess fetal lung fluid.
- 453g of silicone rubber (Dow Corning 3110 RTV mixed with 45 g of S type catalyst) was then injected into the trachea.

- The subject was then placed in the prone position and left for 12 hours for the silicone to cure.
- After drying, the unit was immersed in 10M solution of potassium hydroxide (KOH) for 24 hours to macerate the tissue.
- The cast was then rinsed off under cold running water to remove excess tissue.
- Figure 2.1(a) and 2.1(b) show a lung before and after maceration by KOH [42].

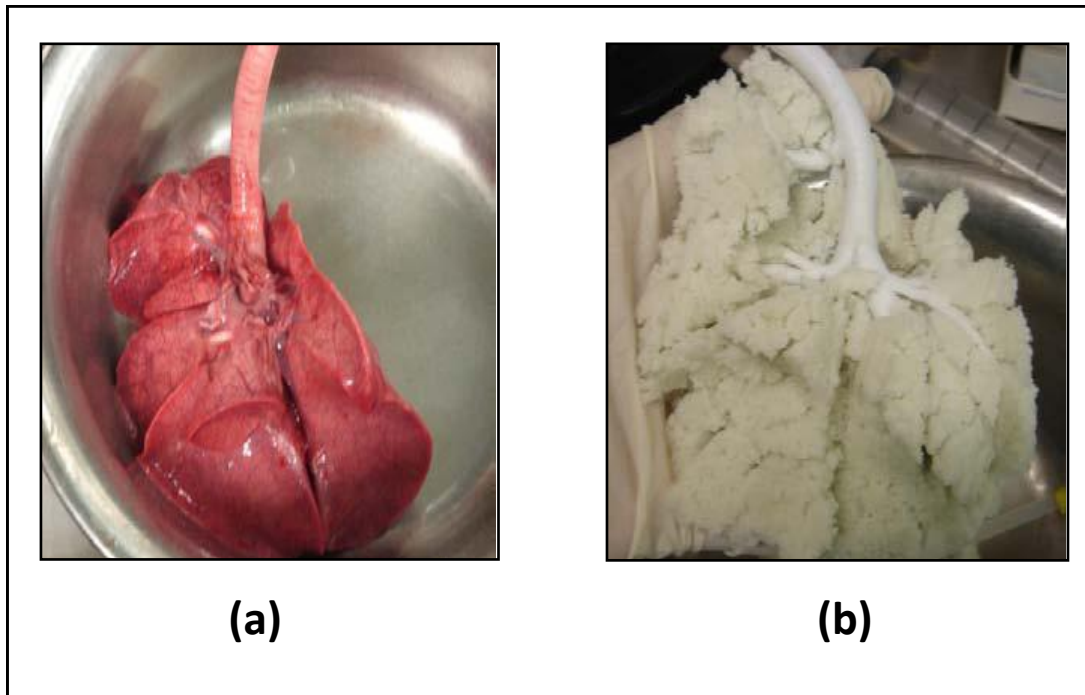


Figure 2.1 Neonatal Lung (a) injected with silicon, (b) after maceration by KOH

2.7.2 Mold Manufacturing

The mold manufacturing process involves the following steps:

- Alveoli (air sacs) were removed gently from the first negative branches (Fig.2.2a).
- The clay foundation was secured in a box made to fit and glued to prevent any silicone leaks (Figure 2.2b).
- The first negative was then immersed half way into 1.5cm thickness of clay formed in the same shape (Figure 2.2b).
- Few holes were placed as keys around the clay to aid with aligning and locking one half of the mold to the other when casting (Figure 2.2b).
- A release agent was applied on the first negative.

Table 2.1 Materials used for positive casting

NAME	QTY/TYPE
Clay	750g
Carton box	1
Glue/ tape	1
Key register	1
Release agent	J-Wax, 400ml
Wax	500g
Vernia	Digital Caliper
Oven	Contherm oven
Stop watch	DSE

- Ultrasil silicone was poured from one corner and allowed to flow naturally, in order to remove the air bubbles, until fully covered. Ultrasil type silicone was chosen because it has the best quality in terms of flexibility and fast curing time in addition to being relatively cheap.
- Once the casted lung was fully covered by silicone, the unit was left for 15 hours to the silicone to cure (Figure 2.2c).
- Once the first half of the silicone mold was cured, the clay was removed from the opposite side (Figure 2.2d).
- The same procedure used for making the second side of molding.
- Figure 2.2e shows both sides fully covered with silicone.
- Figure 2.2f shows the final mold with the original negative cast in between.

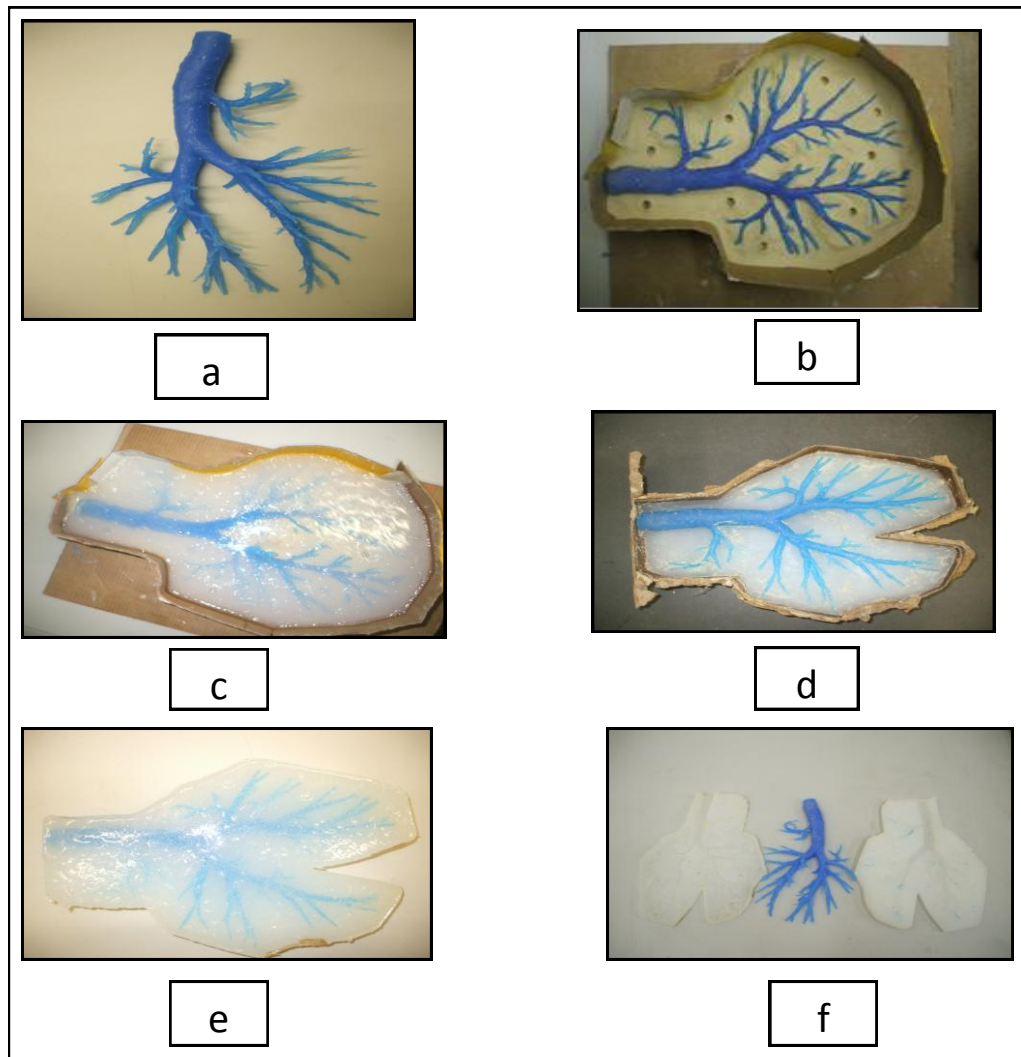


Figure 2.2 Mold manufacturing process

2.7.3 Second Negative

The following procedure was followed to create the second negative.

- The two parts of the mold (Figure 2.2f) were joined together to make one piece.
- The mold was then supported by pieces of carton and taped around to avoid any leaks.
- Wax was melted and poured into the assembled mold.
- The unit was then left for approximately two hours for the wax to dry.
- The mold was opened and the second negative (wax cast) was revealed (Figure 2.3).



Figure 2.3 Second negative embedded into the mold

2.7.4 Final Hollow Airway Cast (Positive Cast)

Dipping, spraying or paintings are commonly used ways of making a cast. Painting the cast is chosen for this work because the Banana-skin silicone is not manufactured in spray mode. In addition the wax is not hard enough to allow dipping in silicone.

The following procedure was used to create the positive cast

- Wax samples (Figure 2.4) were made in order to determine the number of paints required for the desired thickness of each generation.
- Each wax sample was painted with Banana-skin silicone one more layer than the previous wax.
- Each paint thickness was then measured using vernier calipers. Table 2.2 shows the airway generation types and their thickness based on the research finding of Susan et al [43] and how many turns needs to be painted to get that thickness.
- The second negative was painted with the banana-skin silicone repeatedly to obtain the required thickness according to Table 2.2. Figure 2.5 shows the painted airway.
- The painted wax was left for approximately 20 min to dry.
- Once the final paint fully dried, the unit was placed into the Contherm oven at 100⁰ C for 15 min.
- The unit was taken out and squeezed by hand to remove the wax faster.
- The last two steps were repeated until the wax was removed completely.
- The final cast was flushed using hot water to clean the rest of the wax residual. Figure 2.6 shows the final hollow airway cast.

- Figure 2.7 and Figure 2.8 show the schematic diagram of the 142 day and 128 day gestation lamb casts respectively.



Figure 2.4 Painted wax samples

Table 2.2 Airway generation and their thickness

Airway Generation	Thickness(mm)	Number Of Paints
5	0.6	3
4	0.69	4
3	0.85	6
2	1.02	8
1	1.3	10
0	1.38	11

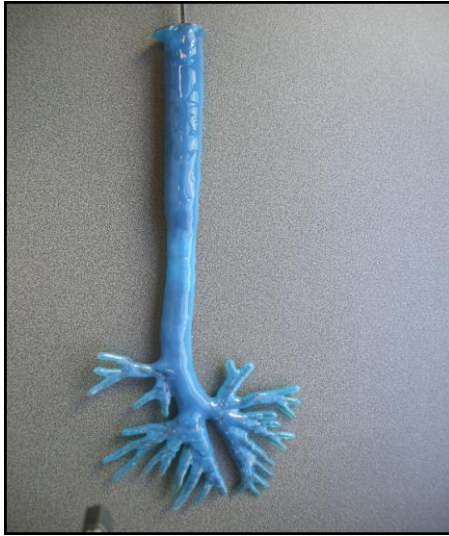


Figure 2.5 Painted negative cast



Fig. 2.6 Final hollow airway cast

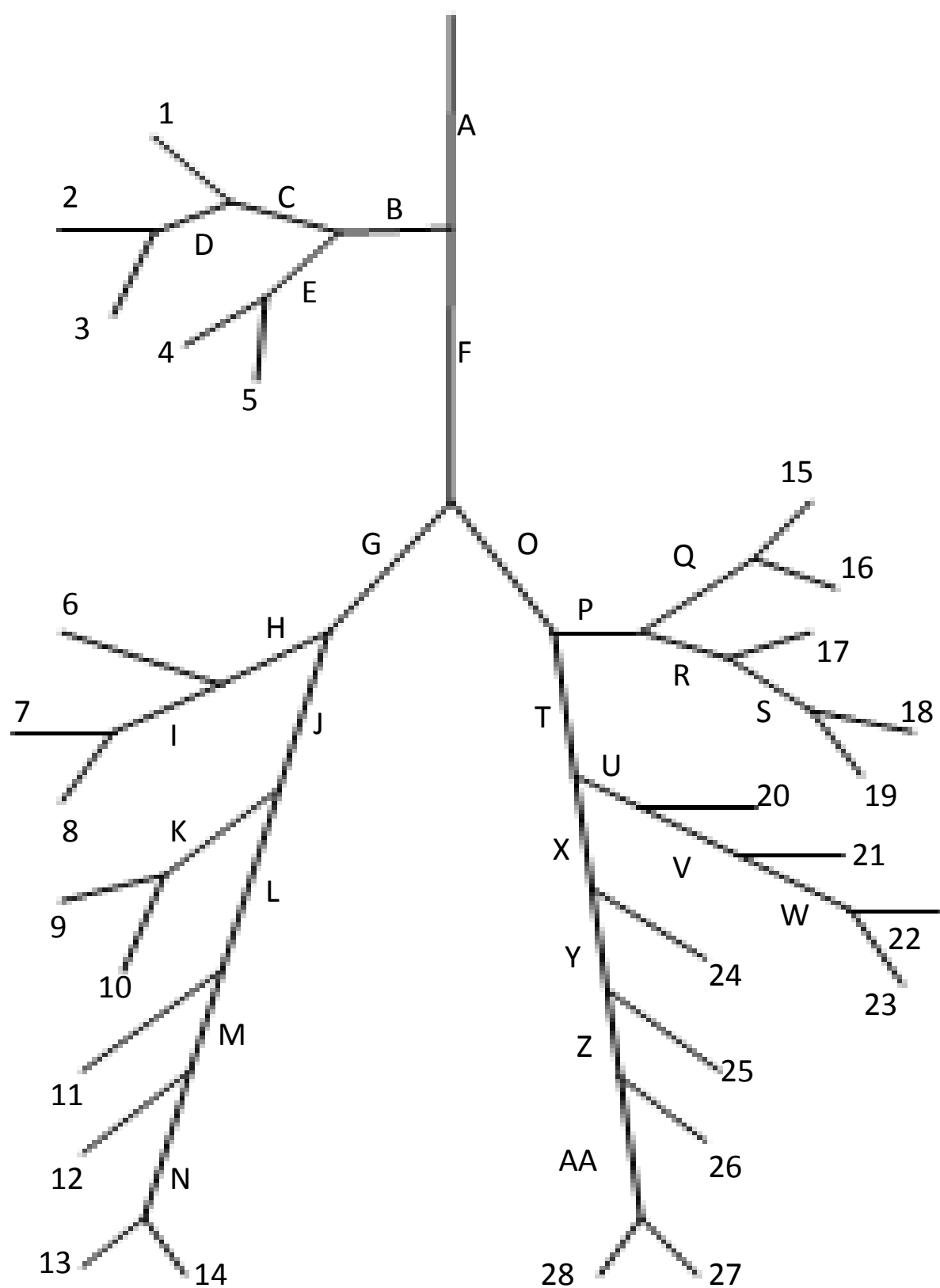


Figure 2.7 Schematic diagram of the 142 day gestation lamb cast

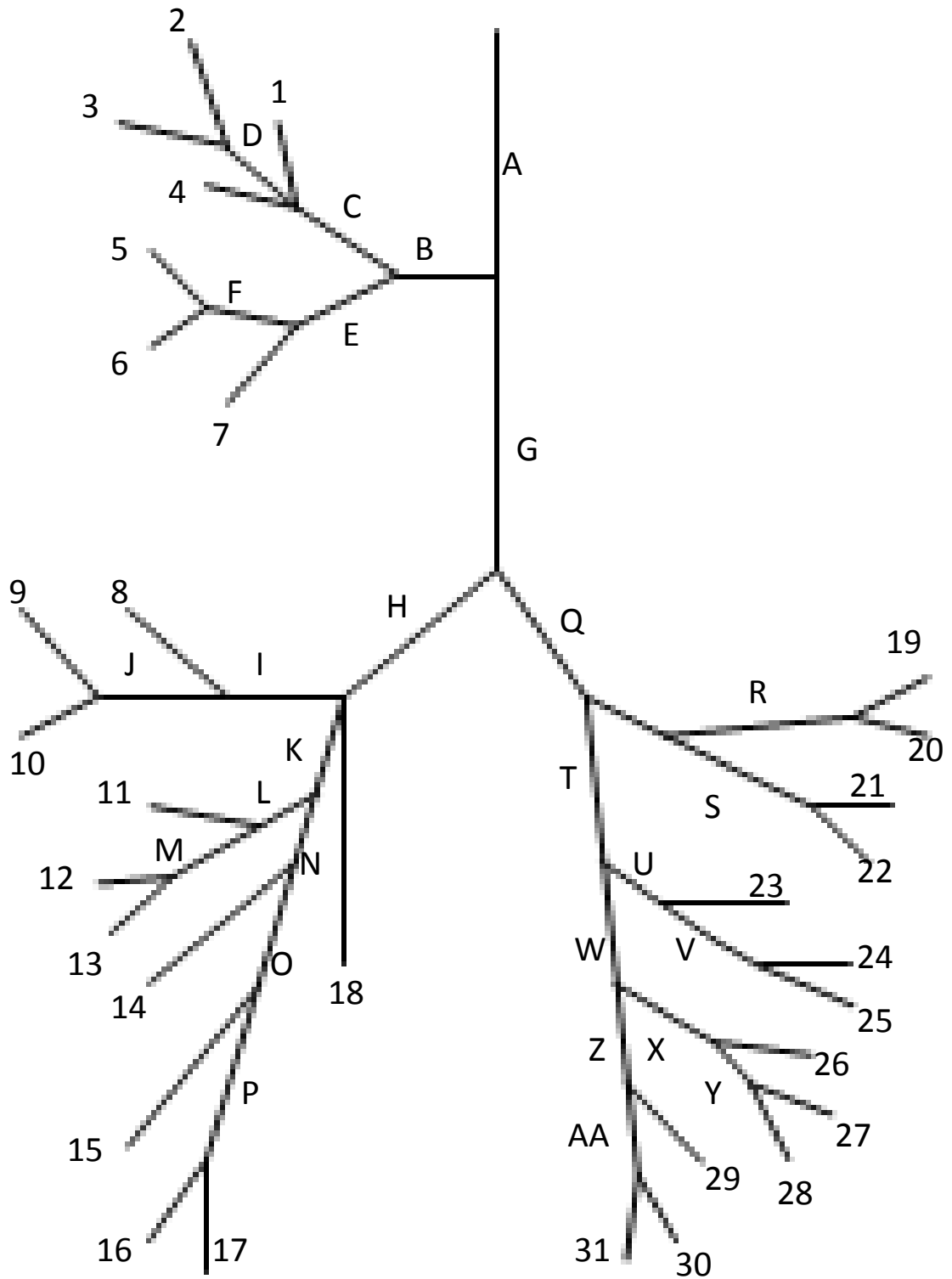


Figure 2.8 Schematic diagram of the 128 day gestation lamb cast

2.8 Closure

The procedure used to develop the final hollow airway casts for the 128 day and 142 day gestation ovine respiratory system have been presented in this chapter. Casting techniques and materials were discussed. Furthermore, the process of making hollow airway casts was described in detail. In the following chapter, the experiments on the casts are presented.

CHAPTER 3

EXPERIMENTAL INVESTIGATION

3.1 Introduction

How far the pressure oscillation frequencies can reach at the bronchi is yet to be determined. This section describes the types of devices used, the experimental setup and the procedure followed in order to measure the pressure oscillation at the smallest bronchi of the casted airway tree.

Adding a displacement encoder to detect the position of the piston in the chamber, a robust safety switches to prevent the collision of the piston with the cylinder's ends and a Labview program for real time data acquisition were added to the existing lung simulator in order to have a complete simple, safe and working simulator.

3.2 Lung Simulator

The existing lung simulator at IBTec is one of the key elements of the experimental section. The aim of the lung simulator is to create a lung environment to imitate the physiology of the human respiratory system. The human respiratory system works through the expansion and contraction of the lungs caused by diaphragmatic movement. The downward and upward movement of the diaphragm shortens or lengthens the chest cavity [1]. This mechanism changes the pressure inside the chest cavity and as a result causes air to flow in or out of the lungs.

The Lung simulator consists of six major components (Figure 3.1); a Chamber, Piston/Cylinder, Displacement encoder, Safety/Limit switches, Motor with encoder and Servo Amplifier.

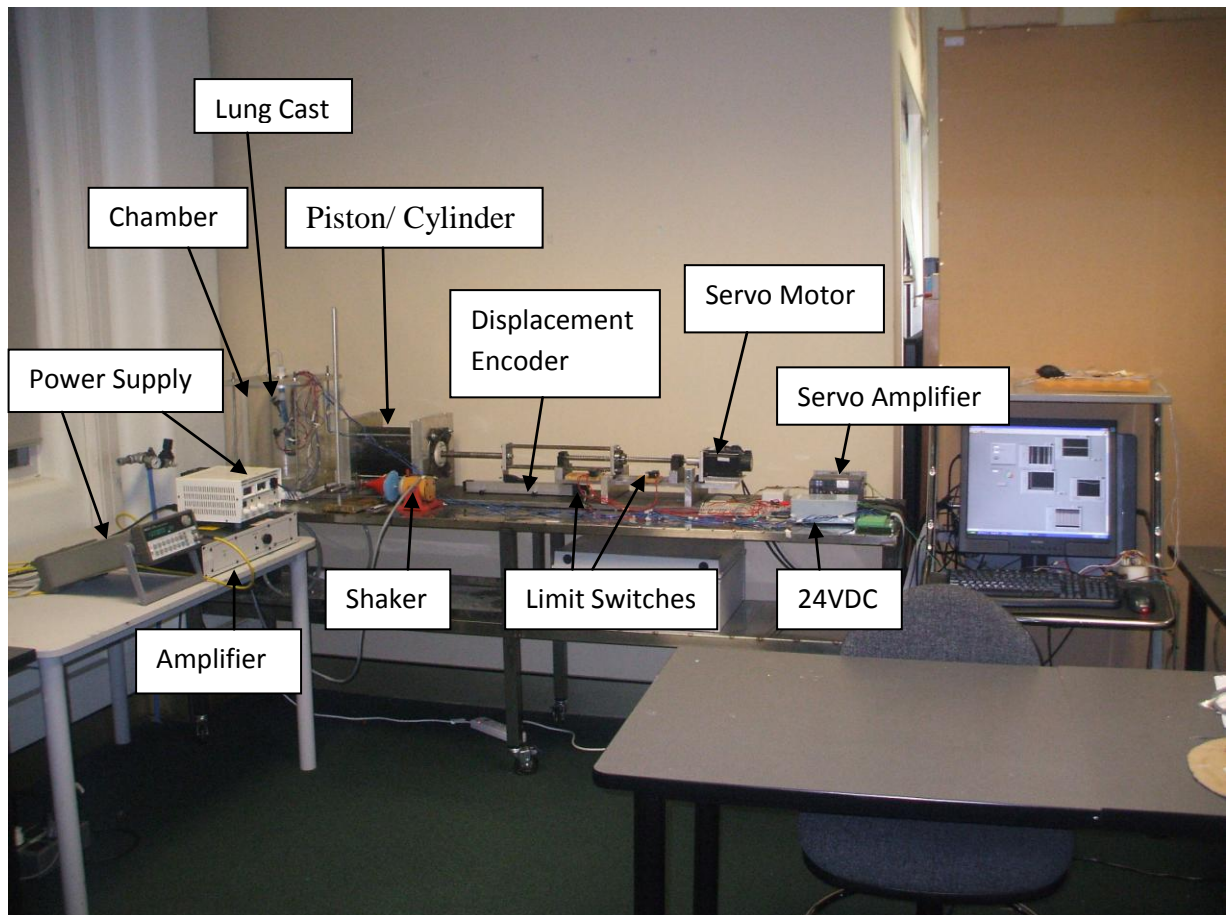


Figure 3.1 Lung simulator setup

3.2.1 Personal Computer

A personal computer is utilized to facilitate the communication between the lung simulator to send the input breathing cycle and to receive the information from all the individual sensors.

The lung simulator is attached to a personal computer through a control system. The real time controller of the entire system has been implemented in the Laboratory Virtual Instrumentation Engineering Workbench (Labview) program. Labview is a visual programming language from National Instruments. It is used for real time data acquisition.

All the measurements fed it through a single data channel. The waveform split function was utilized to separate the data into single entities. The single entities were then converted from a voltage to their proper units.

The lung simulator receives a breath cycle command from the computer using a Labview.

The output signals representing the conditions of the airway pressures are recorded via Labview program and stored on the computer hard disk. Figure 3.2 shows the Labview Block diagram used for this purpose.

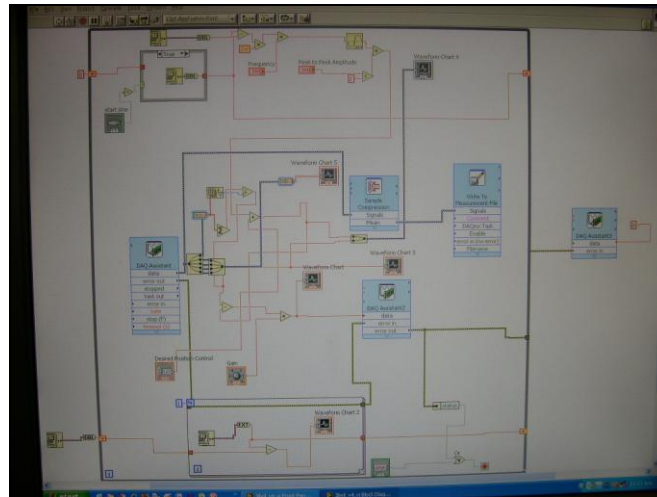


Figure 3.2 Labview Block diagram

For the purposes of evaluation, the measurements were saved to excel file allowing the user to store the necessary measurements that were required for evaluation purpose to a single file called Tests.lvm.

All the measurements were conveyed to the Labview graphical interface, where the data was displayed as a series of graphs. This permits the user to keep track of the system progress allowing the system to be more user-friendly. This was done by connecting the appropriate data signal to a specific X Y graph function block.

3.2.3 National Instruments Extender Board

A National Instruments extender board (Figure 3.3) is used as a link to connect pressure transducers and a displacement encoder to the personal computer as listed in Table 3.1.

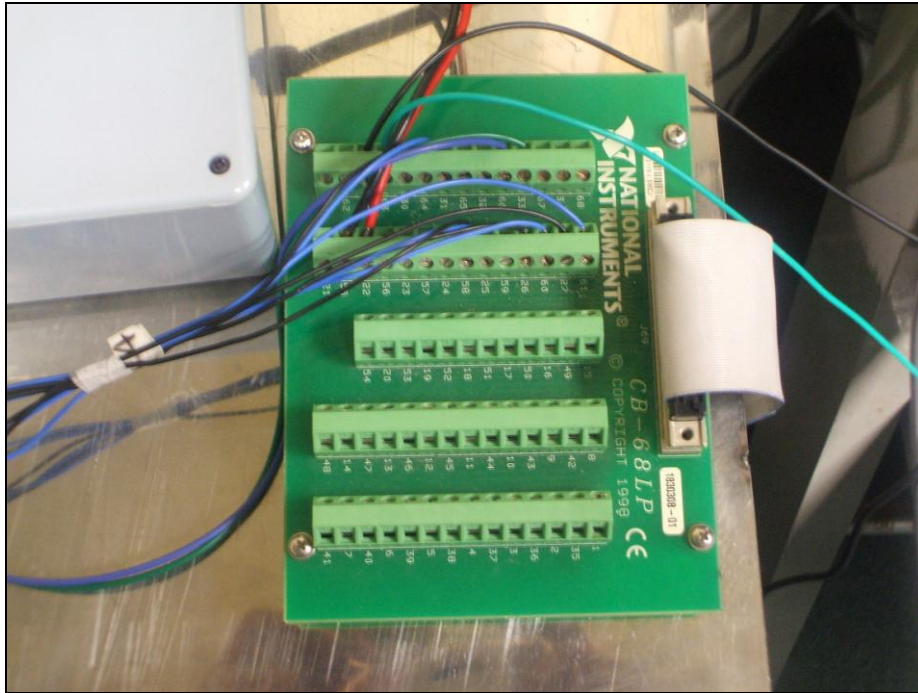


Figure 3.3 National Instruments DAQ Extender board

Table 3.1 Wire and Pin configuration on National Instruments Extender board

Analoge Input/Output	Channel Pin #	Ground Pin #
Displacement	33	66
Pressure Transducer 1	60	26
Pressure Transducer 2	25	58
Pressure Transducer 3	31	64
Pressure Transducer 4	61	27
Control signal	22	55

3.2.4 Fuji Servo System

The Fuji servo system comes with the servo amplifier (Model RYC751D3-VVT2) (Figure 3.4) and the servo motor (Figure 3.5). The servo amplifier has a vibration control function which effectively reduces the mechanical vibration. It also performs auto tuning on the chamber and the servomotor to the optimum setting using the operation pattern in the parameters. Using the control software or the keypad the user can be able to choose and enter the desired function command.



Figur 3.4 Servo Amplifier

3.2.5 Servo Motor

The servo motor (Model GYS751DC2-T2A) is the key element of the lung simulator as it moves the piston inside the cylinder when receiving a command from the servo amplifier which in turn receives its command from the personal computer. Piston movement in the chamber allows the pressure in the chamber to alter causing the lung in the chamber to expand or contract. This process allows the mechanism of exhalation and inhalation to take place.



Figure 3.5 Servo Motor

3.2.6 Pneumatic Cylinder

A pneumatic cylinder (Figure 3.6) is used to force air into the chamber. The pneumatic system is driven by the piston which is moved and controlled by the servo motor. The volume inside the pneumatic cylinder is altered by the movement of the piston which creates the negative pressure with in the chamber. This is the driving force to generate the pressure change and airflow in the tested lung.

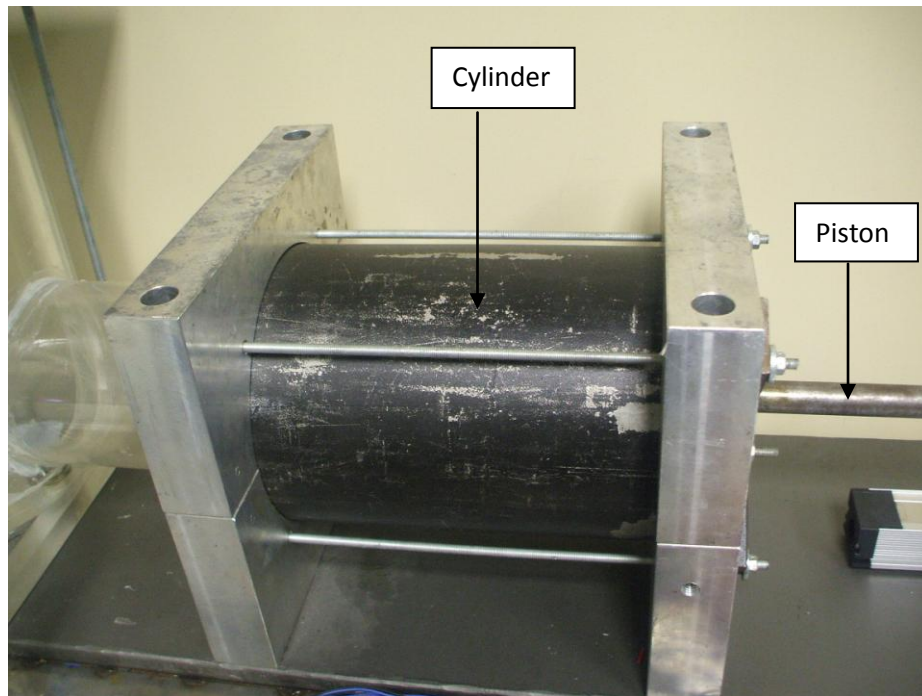


Figure 3.6 Pneumatic Cylinder

3.2.7 Displacement Encoder:

An analogue type MLO-POT displacement encoder (Figure 3.7) from FESTO is used in this project to detect the position of the piston in the chamber. It is an analogue displacement encoder with high resolution, high speeds of travel and long service life. The piston position is then measured using this encoder and used as a feedback to determine the pattern of the breath cycle.

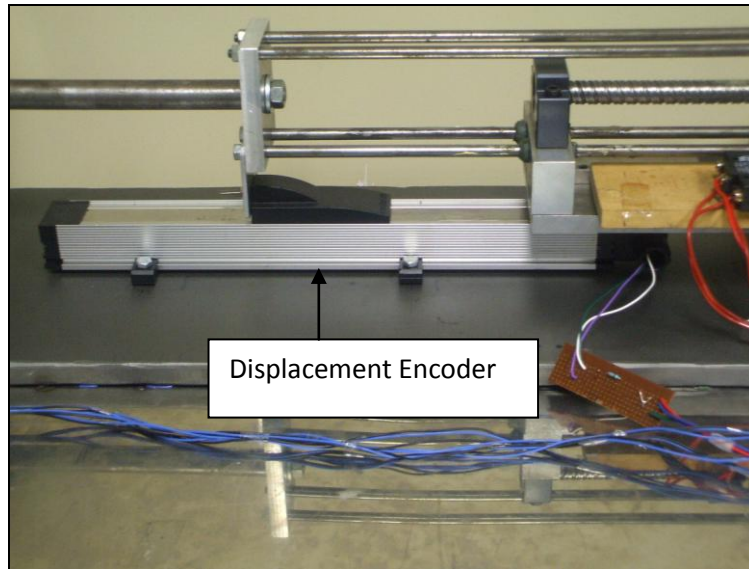


Figure 3.7 Displacement Encoder

3.2.8 Safety Mechanism

The existing lung simulator at IBTec did not have a hardware controlled safety mechanism that prevents the collision of the piston with the cylinder's ends. Two limit switches (Figure 3.8) were placed in a position where the piston can move adequate distance to generate the required lung volume in the chamber. Additional software safety mechanism was also maintained using Labview program to control the piston from striking the cylinder ends. The switches were mounted on wood using heavy-duty double side tape to hold in its proper position.

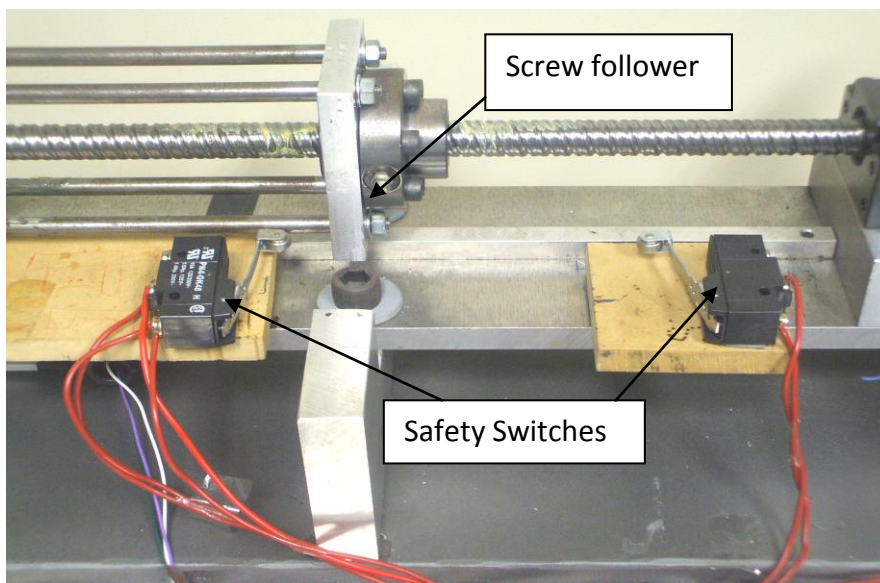


Figure 3.8 Safety switches

3.2.8.1 Safety switches

Figure 3.8 shows two safety switches from (PN4-GK48, Sicatron) which determine the precision switching characteristic which is used to spot the position of the piston. When the screw follower makes contact with the safety switch, it causes the 24V DC power rail for the motor's controller to be switched off causing the motor to stop instantly. The advantage of this was that the system was controlled physically to prevent any undesirable action.

3.2.8.2 Relay:

An Electromechanical relay (G2RL-1E 24DC, Omron) (Figure 3.9) was part of the safety mechanism system. Relays are generally used to switch a system on and off. Once the screw follower comes in contact with the safety switch, the relay coil is energized then it induces a magnetic field that moves the armature to open the normally closed contact causing the power supply to be cut off, thereby causing the motor to be stop.

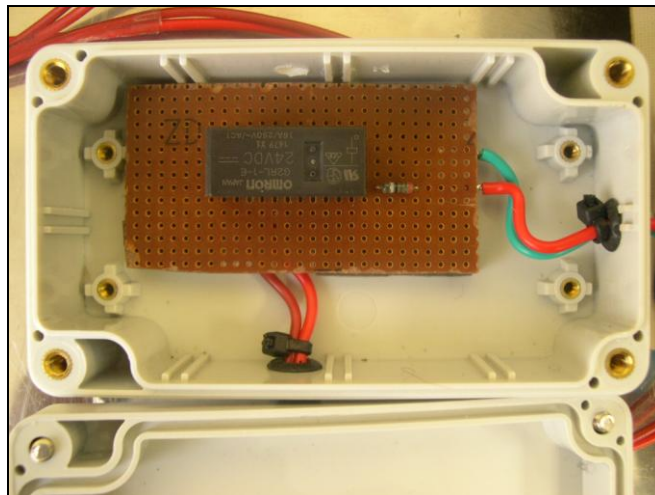


Figure 3.9 Relay

3.3 Airway Tree Setup

The casted airway tree (Figure 3.10) was suspended inside the lung simulator chamber and taped at the chamber inlet in order to avoid air leaks. Pressure transducers were attached at different positions on the branches of airway. A separate hole was made in the chamber to facilitate access to the measuring wires. A tube was attached between the top of the trachea and the flow meter in order to measure the airflow.

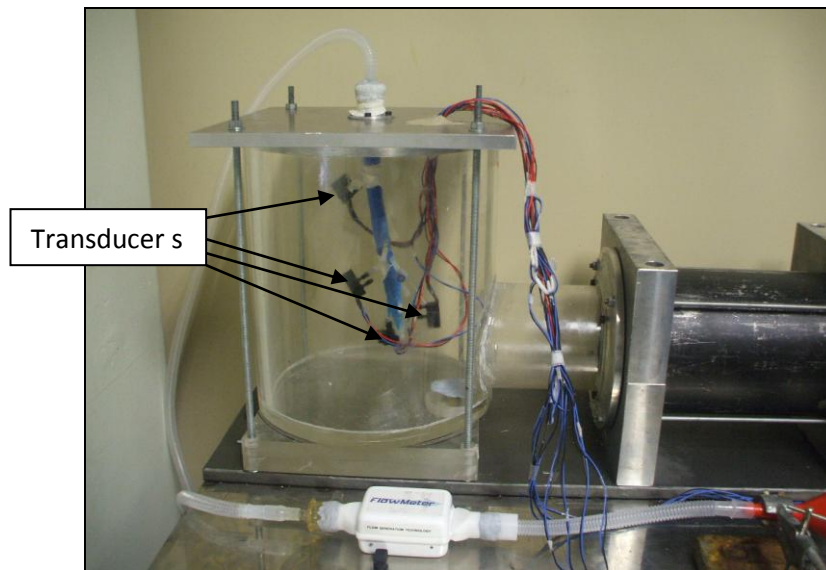


Figure 3.10 Casted airway suspended in the Chamber

3.4. Pressure Measurement

There were several criteria listed to select the best pressure sensor. The first criterion was the pressure range. Achievable mean pressures that the Bubble CPAP system can create are from 3 - 10 cmH₂O [44]. Considering this as an input, in order to measure the pressure at far end of the bronchi, it requires a sensor with operation pressure lower than 3cmH₂O. The second criterion was port diameter. Further down the airway tree the diameter of the bronchi is far smaller than the trachea. Therefore port diameter of the sensor need to be smaller in order to insert it into those bronchioles. And also the effect of the pressure sensor on the bronchi themselves needs to be kept to a minimum so that the pressure sensor does not affect the acoustic propagation when it is inserted. Sensitivity also considered as the sensor must measure the pressure without any significant delay between the output signal and the real time data. Table 3.2 compares some of the pressure sensors that considered for this work. 1 Inch-D-4V found the best option with the time and finance constrain we had.

Differential pressure transducers (1 INCH-D-4V, All Sensors) were utilised to measure the changes to the pressure at the desired locations on the airway tree (Figure 3.11). The sensor uses silicon, and is micro machined to provide a very linear output to measured pressure. It was designed to reduce output offset error due to change in temperature and position sensitivity.

Supplier	Part Num	Price	Pressure Range	Outputs	Port Dia(mm)	Sensitivity	Response Time
Honeywell	163PC01D48	\$197.49	-7.87 to 47.24 inH2O	1-5v	5	0.36 V/in H2O	1ms
Honeywell	26PC0350D6J	25EUR/chk	0 to 6920 inH2O	16.7mv	1.78		1ms
Honeywell	ASCX30AN	\$288.42	0 to 830.4 inH2O	4.5V	2.67	0.15V/psi	100 us
Honeywell	XCAL4004D	\$280.33	0 to 4 inH2O	4V	4.8	0.5 V/in H2O	
Honeywell	164PC01D76	\$359.70	0 to 5 inH2O	1-6V		1V/in H2O	1ms
ALL Sensors	20-INCH-D-MV	\$55.50	0 to 20 inH2O	20mv	4.8	±5uv	<100us
ALL Sensors	5 INCH-D2-BASIC	\$37.50	22.4 inH2O	0-22.5mv	2.14	±15uv	<100us
ALL Sensors	20-INCH-D1-BASIC	\$37	0 to 20 inH2O	30mv	2.14	±5uv	<100us
ALL Sensors	20-INCH-G-4V	\$82.50	0 to 20 inH2O	4v	4.8	±5mv	<500us
ALL Sensors	1 INCH-D-4V	\$110	+/-1 inH2O	0.25-4.25V	4.4	±5mv	<500us

Table 3.2 List of Pressure Sensors

Four pressure transducers were inserted at different locations on the airway tree to measure the pressure change. Two fixed locations, one transducer at the inlet and the other at the lower trachea. During the test the other two transducer locations were changed to different bronchi locations in order to compare individual bronchi pressure to the trachea.

All transducers were connected to the data acquisition extender board as shown in Figure 3.3; pin and wire configurations are shown in Table 3.1.

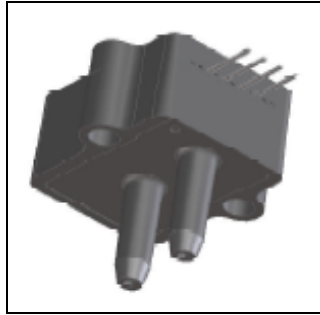


Figure 3.11 Pressure Transducer

3.5. Flow Meter

The VenThor Model flowmeter from Wavefront was used to measure the total flow in and out of the airway cast. The accuracy of the flow meter is 3% and designed for a flow range of +/- 8L/sec. Figure 3.12 shows the picture of the flow meter used.



Figure 3.12 Flow meter

3.6. Shaker

A permanent magnet shaker (V101/3 Ling Dynamic Systems (LDS), USA) is designed to produce a pressure oscillation (Figure 3.13). The magnet shaker has a light weight moving armature which has been optimized to supply a wide frequency range. It is driven by a function waveform generator (Model 33120A, Hewlett Packard, USA) via an amplifier

(PA25E, LDS, USA). The power amplifier is used to extend the usable frequency range of the shaker and can achieve up to 8.9 N peak sine force.

A shaker was introduced instead of the Bubble CPAP in order to apply a signal that contains all frequencies in equal amounts. These signals were proven to be useful test signal to verify the frequency response of non-linear systems [100]. Under normal operating conditions, the range of frequencies present in the Bubble CPAP system is 10-70Hz [42] so the shaker is used to deliver the waveforms to simulate these breathing frequencies.

The shaker was connected to a cone that was made out of plastic. The purpose of the cone was to reproduce or extend the frequency response that was generated by the shaker.

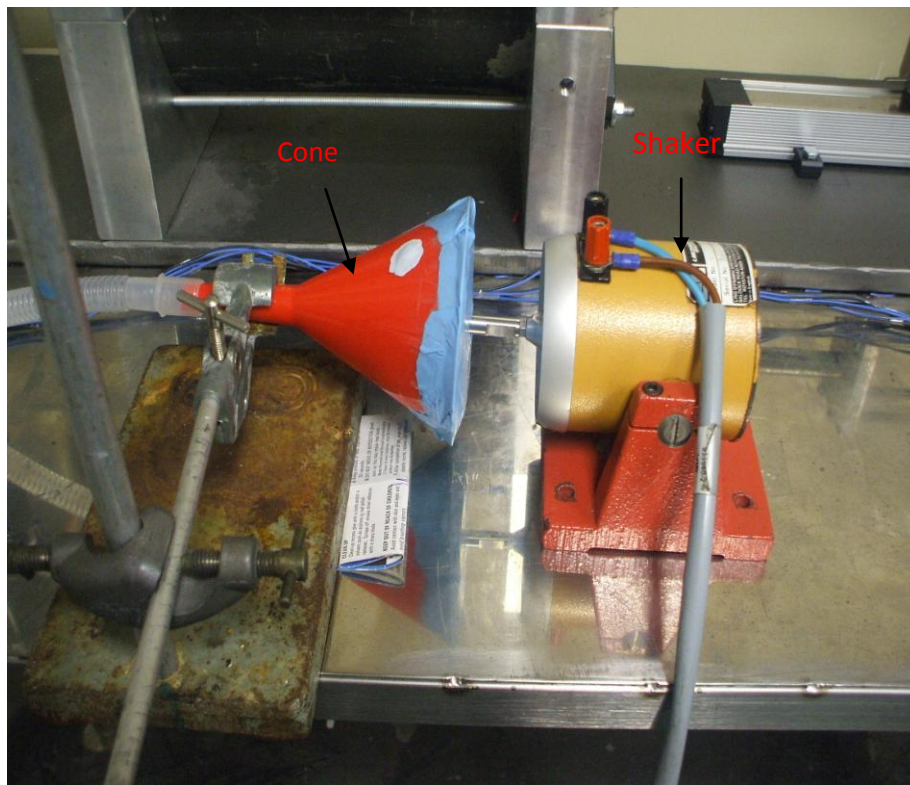


Figure 3.13 Shaker with cone

3.7 Experimental Procedure

The following procedure was set for each operation.

- a) The airway tree cast was suspended and sealed in the chamber so that all the supplied air flows through it. The pressure transducers were attached at the trachea, lower trachea and bronchi locations of the airway tree.

- b) Pressure transducer wires were connected to the appropriate pins on the NI extended board as indicated in Table 3.1.
- c) The flow meter was connected between the airway tree cast and the shaker using plastic tubes.
- d) The PA25E Amplifier was connected to the shaker and its value set to a constant limit of 1.5.
- e) The amplifier was supplied with different frequencies from 10Hz to 80Hz using the HP-33120A Function Waveform generator. The amplitude of the waveform was set at two levels, which was 0.5V and 1V in order to record more data and analyze its effect on the pressure oscillation amplitude at the end of bronchi.
- f) Parameter editing mode which is “Pn01” selected by pressing the “Mode” key at servo amplifier using the keypad and the LCD display. Then press and hold the “Enter” key to go to parameter editing sub division mode and choose “no03”. Then press and hold the “Enter” key again to choose class 1.
- g) The device number and the channel as stated in Table 3.1 were entered into the Labview program DAQ assistant. Sampling rate was set to 10 KHz.
- h) For each experiment, 20 seconds of data was acquired using the different combination of tests as detailed in Table 3.2.

The approximate respiratory rates for 146day and 125 day gestation lambs are 0.5b/sec and 0.67b/sec respectively [45, 46]. 0.55b/sec respiratory rate added to the list in order to perform more analysis. Controlling the respiratory rate and the airflow amplitude were performed using the lung simulator and the shaker respectively.
- i) The next step was transforming the recorded data into the frequency domain in order to obtain a frequency analysis. A Fast Fourier Transform (FFT) algorithm was applied (see Appendix A) and a useful signal power against frequency plot for each experiment was obtained.
- j) Each plot magnitude was normalized by giving the signal power with the highest magnitude a value of one. In this case the highest value was at the trachea so it has a value of one and the rest of the values were relative to the Trachea magnitude. The plot was then exported to Excel for further analysis.

Table 3.3 - Experimental Parameters for each branch

Frequency(Hz)	Air Flow Amplitude(V)_Respiratory Rate(b/sec)					
	0.5_0.5	0.5_0.55	0.5_0.67	1_0.5	1_0.55	1_0.67
10	10_0.5_0.5	10_0.5_0.5 5	10_0.5_0.67	10_1_0.5	10_1_0.55	10_1_0.67
20	20_0.5_0.5	20_0.5_0.5 5	20_0.5_0.67	20_1_0.5	20_1_0.55	20_1_0.67
30	30_0.5_0.5	30_0.5_0.5 5	30_0.5_0.67	30_1_0.5	30_1_0.55	30_1_0.67
40	40_0.5_0.5	40_0.5_0.5 5	40_0.5_0.67	40_1_0.5	40_1_0.55	40_1_0.67
50	50_0.5_0.5	50_0.5_0.5 5	50_0.5_0.67	50_1_0.5	50_1_0.55	50_1_0.67
60	60_0.5_0.5	60_0.5_0.5 5	60_0.5_0.67	60_1_0.5	60_1_0.55	60_1_0.67
70	70_0.5_0.5	70_0.5_0.5 5	70_0.5_0.67	70_1_0.5	70_1_0.55	70_1_0.67
80	80_0.5_0.5	80_0.5_0.5 5	80_0.5_0.67	80_1_0.5	80_1_0.55	80_1_0.67

3.8 Closure

The experimental setup and procedure have been presented in this chapter. The experimental results generated in this chapter and the modelling results from next chapter are listed in Chapter 5. Modelling of the system is presented in the following chapter.

CHAPTER 4

MODELLING

4.1 Introduction

This chapter begins by describing the modelling system, which is chosen for comparison with experimental data (section 4.2). Section 4.3 then lists the model assumptions while section 4.4 describes model development. Section 4.5 explains the Simulink modelling which is required to change the mathematical equations into a computational model. Section 4.6 closes the chapter.

4.2 Modelling system

The theoretical modeling of the work was based on proven work conducted at IBTec [42] and modified to suit the current application. It is the closest modelling result available, which can be used to compare to experimental results. It describes a more descriptive multi-compartmental lung model and investigates the effect of pressure oscillations on respiratory system performance. The study proved that certain frequencies can reach as far as the alveoli and have the effect on of achieving a better performance of the neonatal lung. A brief summary of the system development is given as follows.

The lung is defined as a system of branched airways, consisting of 12 airways including the trachea and bronchi as well as 5 separate lobes present in the actual lung, Figure (4.1). Airway pressures, flow rates and volumes were the outputs of the model at the airway opening and at the individual lobes. These are used to calculate the work of breathing (WOB) at each location as a measure of respiratory performance.

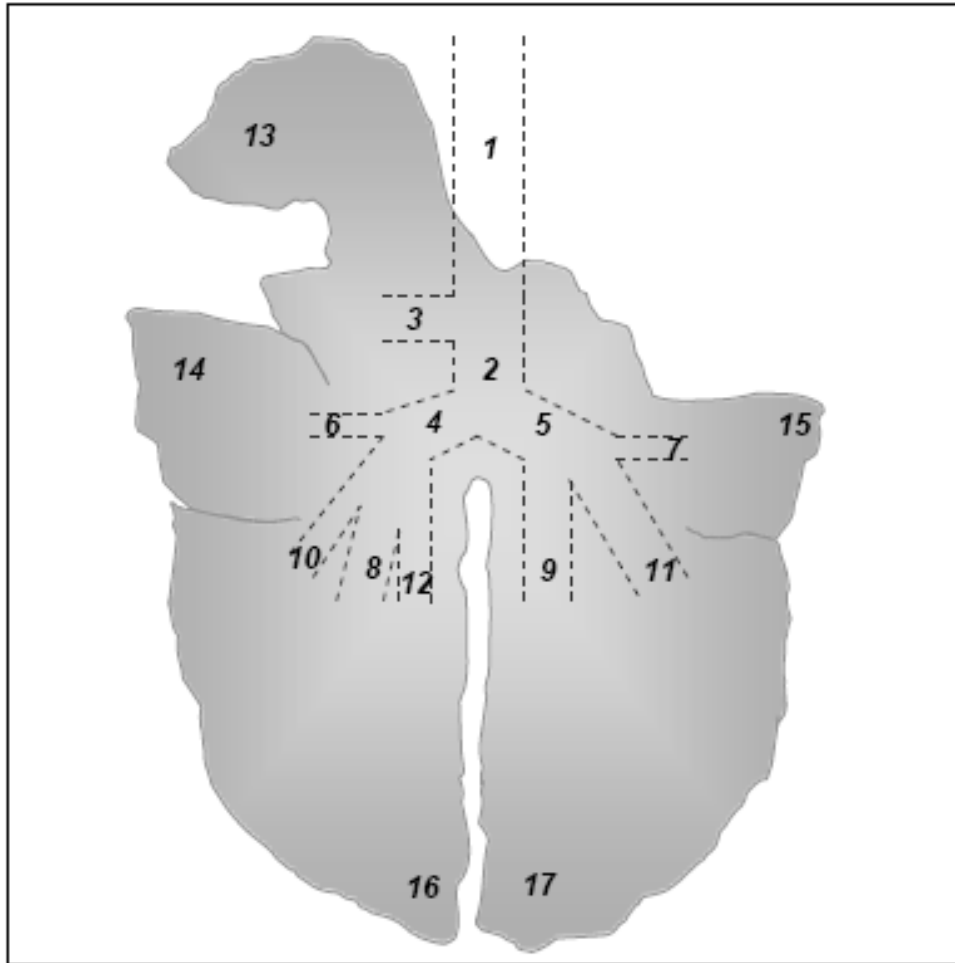


Figure 4.1 The elements of the ovine respiratory system model[42]

4.3 Model Assumptions

As some relationships were undefined or uncharacterised for premature lung in the literature, the following assumptions were made for this level of investigation.

- Humidity effects are neglected and used a constant temperature of 39°C (312 K) i.e lamb rectal temperature.
- Ideal gas is assumed and gas compressibility is neglected.
- The airways are assumed to be straight with constant circular cross-section.
- Pressure variations in sections 1-12 are also very small and can be ignored as it is very short.
- The walls of sections 1-12 are considered to be rigid as it contains varying amounts of cartilage.

4.4 Model Development

Some of the equations used to calculate various properties are mentioned below:

Ideal gas equation used to calculate the rate of change of pressure:

$$P_{\text{section}} V_{\text{section}} = m_{\text{section}} RT \quad (1)$$

Where: P_{section} is the absolute pressure within the section (Pa)

V_{section} is the volume of the section (m³)

m_{section} is the mass of air in the section (Kg)

R is the specific gas constant of air at 312K (Pa.m³/(Kg.K))

T is the temperature in Kelvin (K)

If we consider a time varying pressure in any particular section, equation (1) becomes

$$\frac{d(P_{\text{section}} V_{\text{section}})}{dt} = \frac{d(m_{\text{section}} RT)}{dt} \quad (2)$$

Assuming V_{section} , R and T constant, equation (2) becomes

$$\frac{dP_{\text{section}}}{dt} = \frac{RT}{V_{\text{section}}} \frac{dm_{\text{section}}}{dt} \quad (3)$$

Applying the conservation of mass to a section gives the change in the mass of air in that section, $\Delta m_{\text{section}}$. This can be written as

$$\Delta m_{\text{section}} = m_{\text{in}} - m_{\text{out}} \quad (4)$$

Where m_{in} is the mass that enters the section and m_{out} is the mass that leaves the section. For a time varying system,

$$\frac{dm_{\text{section}}}{dt} = \frac{d}{dt}(m_{\text{in}} - m_{\text{out}}) = \dot{m}_{\text{in}} - \dot{m}_{\text{out}} \quad (5)$$

Equation (3) can now be written as

$$\frac{dP_{section}}{dt} = \frac{RT}{V_{section}} (\dot{m}_{in} - \dot{m}_{out}) \quad (6)$$

Applying equation (6) to Upper Trachea (for example) gives:

$$\frac{dP_{up\ trachea}}{dt} = \frac{RT}{V_{up\ trachea}} (\dot{m}_{up\ trachea} - \dot{m}_{mid\ trachea}) \quad (7)$$

for the upper trachea, where

$$\dot{m}_{mid\ trachea} = \dot{m}_{low\ trachea} + \dot{m}_{R\ api} \quad (8)$$

The mass flow rate determined using empirical relations which is developed by Reynolds and Lee[47]

$$\Delta P_{section} = (a + b Re) \Delta P_{poiseuille} \quad (9)$$

Where a and b are scaling coefficients as defined by Reynolds and Lee.

$$\Delta P_{poiseuille} = \frac{128 \mu L_{section}}{\pi D_{section}^4 \rho} \dot{m}_{section} \quad (10)$$

Combining equations (8) and (9)

$$\dot{m}_{in} = \frac{\Delta P_{section}}{(a + b Re)} \frac{\pi D_{section}^4 \rho}{128 \mu L_{section}} \quad (11)$$

$D_{section}$: Diameter of the section

$L_{section}$: Length of the section

$\dot{m}_{section}$: Mass flow through the section

μ and ρ : Dynamic viscosity and density respectively

The mass flow rate in the upper trachea is

$$\dot{m}_{\text{up trachea}} = \frac{P_{\text{interface}} - P_{\text{up trachea}}}{(24 + 0.0162 \text{Re})} \frac{\pi D_{\text{up trachea}}^4 \rho}{128 \mu L_{\text{up trachea}}} \quad (12)$$

4.5 Simulink Model

Simulink is a graphical user interface block diagram simulator. It is used for modelling and analysing a system. The Simulink model was developed by Reddy [42] using the equations mentioned earlier. This model is able to predict the pressure, flow rate and volume of each lobe and airway section. Separate models were formulated for 128 day and 142 day gestation lambs. Each model used to have 3 main sub-systems, which were the tracheo-bronchial subsystem, the viscoelastic subsystem and the respiratory support device subsystem. The Viscoelastic and the Respiratory device sub-system are removed as it is not required for the current work.

The pressure conversion system is added as it was required in order to convert the experimental data from cmH₂O to pascals and then to absolute pressure in order to match the units of the original Simulink model. Figure 4.2 and Figure 4.3 shows the picture of the Airways subsystem and the overall Simulink Model respectively.

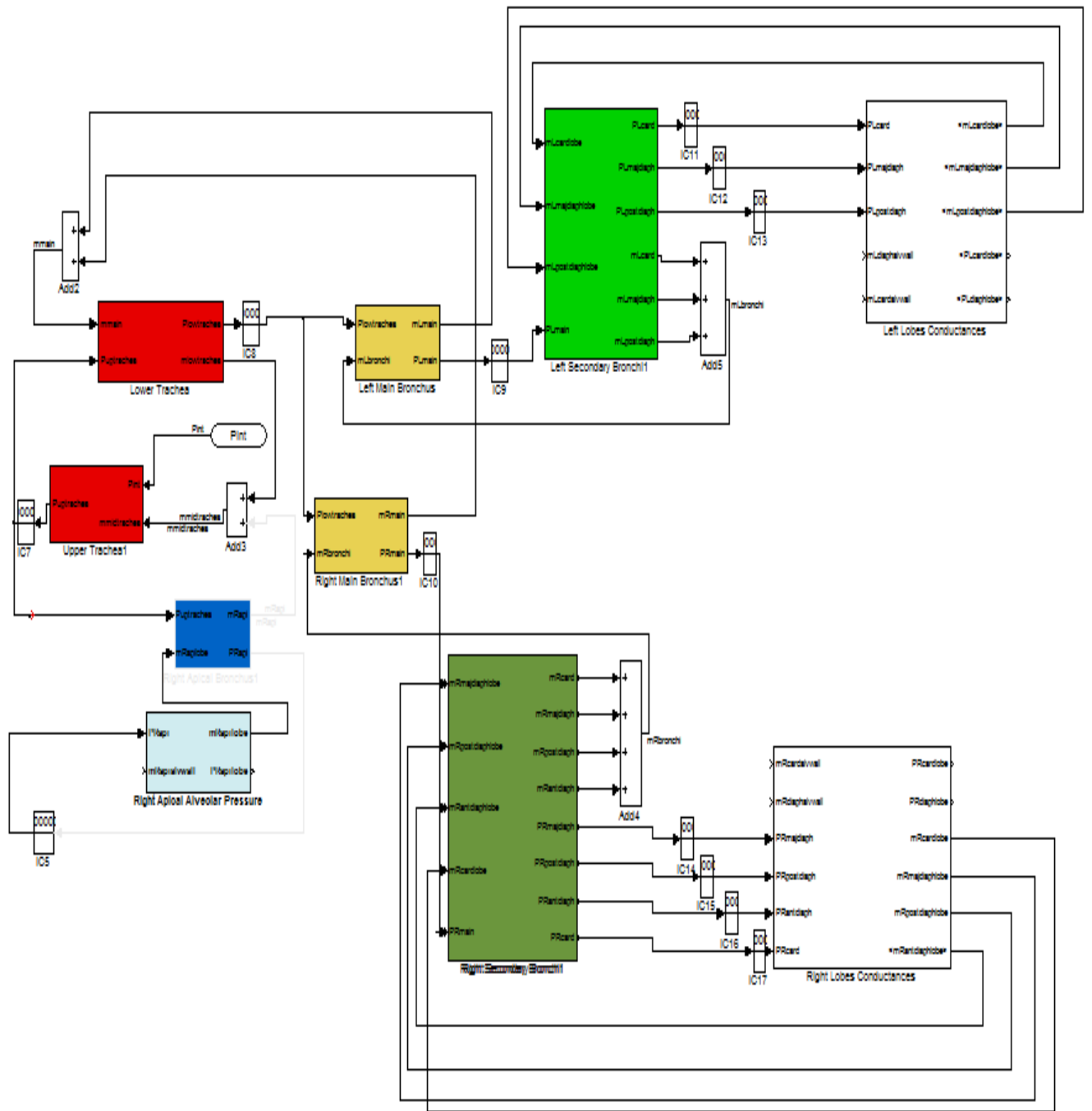


Figure 4.2 Airways Subsystem [42]

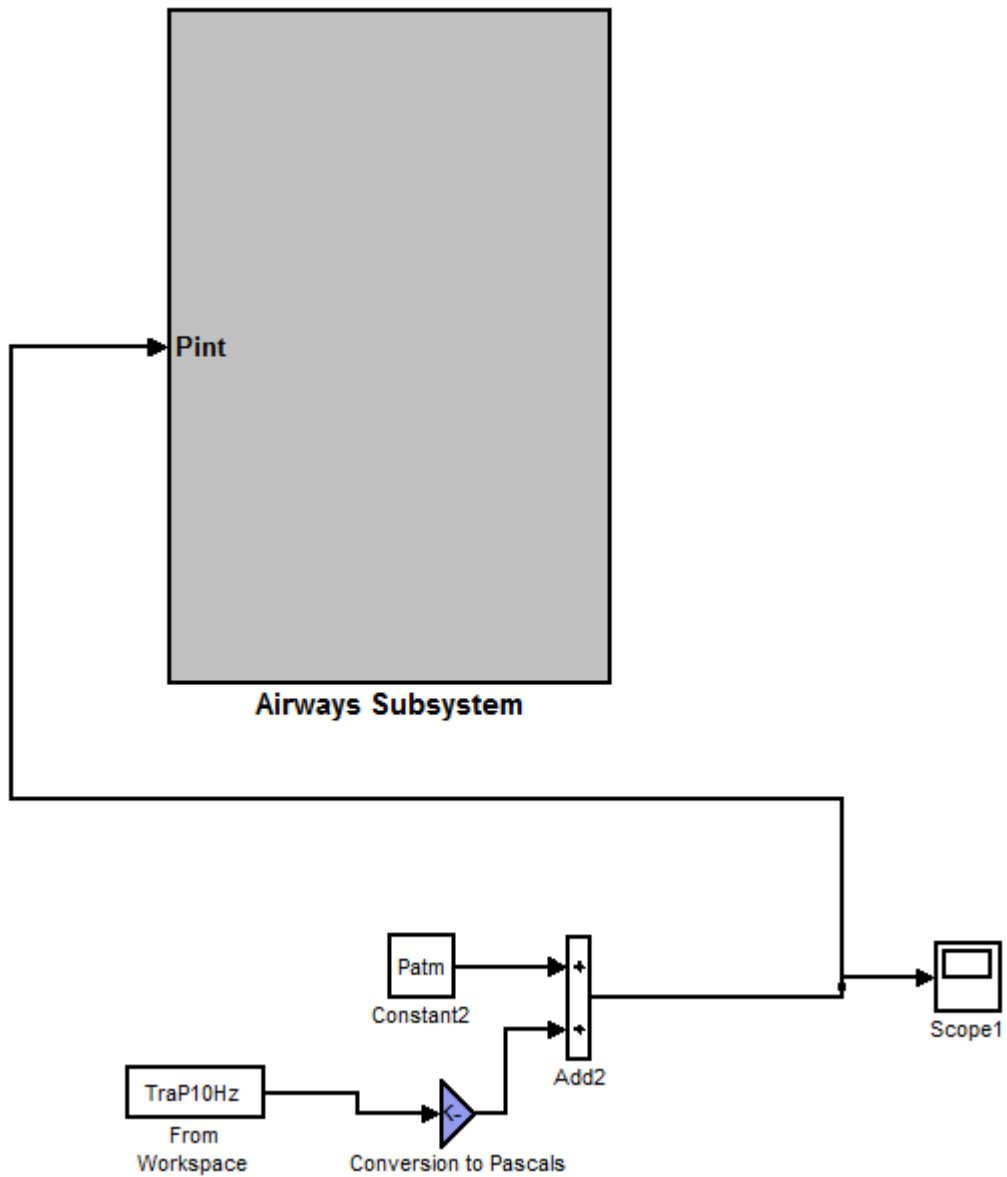


Figure 4.3 Overall Simulink Model [42]

4.6 Closure

The modified model above was used to compare the experimental result presented in chapter 3. The modelling and the experimental results are presented in the following chapter.

CHAPTER 5

RESULTS

5.1 Introduction

This section covers results of both casted airways. The results are obtained after the Fast Fourier Transform analysis performed. This identifies the frequencies of pressure oscillations and their magnitude at different locations in the casted airway trees. Two pressure transducers were used at fixed locations, one transducer at the inlet (Trachea) and the other at the lower trachea. The other two transducers were changed to different bronchi locations in order to compare individual bronchi pressure to the trachea. As a result the experimental outcome listed pairing two bronchi locations. Section 5.2 describes the test result obtained from the 142 day gestation lamb. It summarizes the main results in terms of oscillation amplitudes at each bronchi. Section 5.3 likewise summarizes the 128 day gestation lamb result. Section 5.4 describes the test result obtained from the modeling system.

5.2 Airway Tests on 142 day lung cast

This section includes the test result from the 142 day gestation lamb airway tree cast. The test process was done as outlined on the test procedure using the different combination respiratory rate and airflow amplitude. Those are listed in Table 3.2. Figure 5.1 to Figure 5.4 show the frequency spectrum of pressure oscillations and their magnitude for each particular position at the casted airway tree.

5.2.1 Bronchi #4 and #19

Figure 5.1 shows the pressure ratio analysis of the Lower Trachea (LT), Bronchi #4 and Bronchi #19 against Trachea (T). Increasing the respiratory rate shows an overall decrease in the frequency amplitude at Lower Trachea and Bronchi across all the frequencies. It shows distinct and strong spikes at the Bronchi around 40Hz and 60Hz with the airflow amplitude of 0.5V. Frequency power at all airways observed to decrease with increased airflow amplitude. A moderate spike observed to appear at 20Hz at 1V airflow amplitude and 0.55b/sec respiratory rate. Increasing the airflow amplitude shows decrease in the frequency power at the Bronchi.

5.2.2 Bronchi #6 and #21

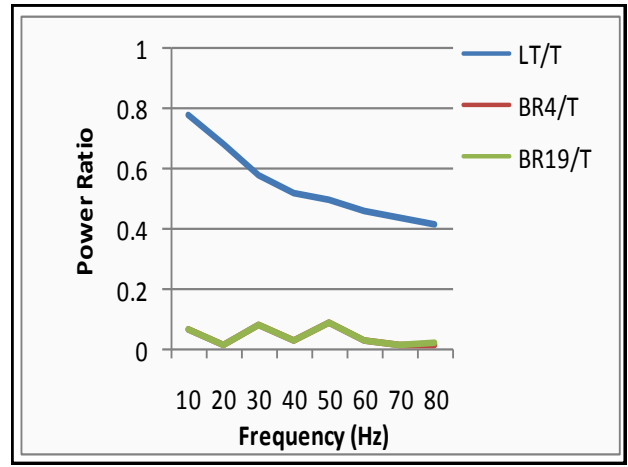
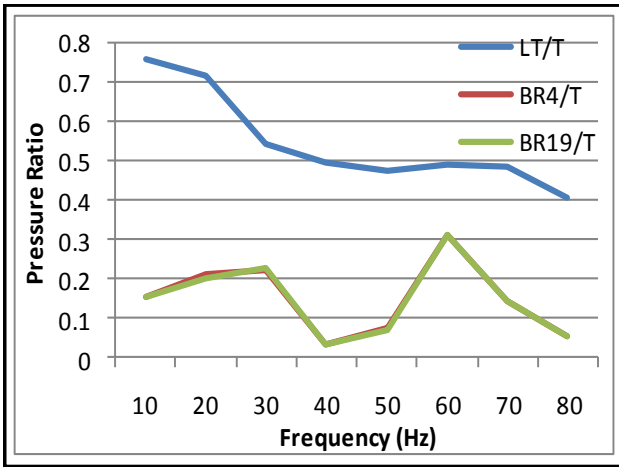
The result in Figure 5.2, which is pressure ratio analysis of the Lower Trachea (LT), Bronchi #6 and Bronchi #21 against Trachea (T), shows a distinct and strong spikes at the Bronchi and Lower Trachea around 40Hz at 0.5V Airflow amplitude and 0.5b/sec Respiratory rate. Generally, increasing the airflow amplitude shows decrease in the frequency amplitude at the bronchi. When the respiratory rate increased to 0.55L/sec, spikes with moderate amplitude of 0.6 appeared at Lower Trachea at 40Hz. Frequency oscillation amplitude at the Lower trachea and Bronchi observed to decrease when the respiratory rate increased to 0.67L/sec.

5.2.3 Bronchi #9 and #23

The pressure ratio analysis of the Lower Trachea (LT), Bronchi #9 and Bronchi #23 against Trachea (T), Figure 5.3, shows a slight decrease in Frequency power at Bronchi when the airflow amplitude increased. A moderate spike between 0.3 and 0.5 was observed at Bronchi at frequency of 30Hz, when the respiratory rate increased. Increasing the airflow amplitude didn't show any significant change in frequency power at the Bronchi. At 0.55L/sec respiratory rate, there was a very distinct and strong spike around 30Hz. Increasing the respiratory rate shows a slight decrease in the frequency amplitude at Bronchi across all the frequencies.

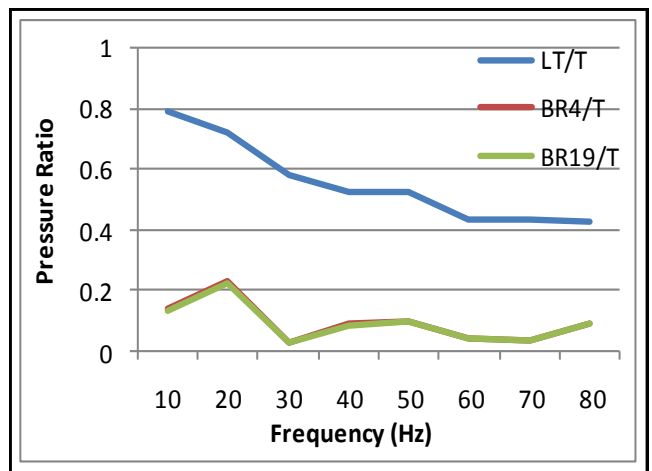
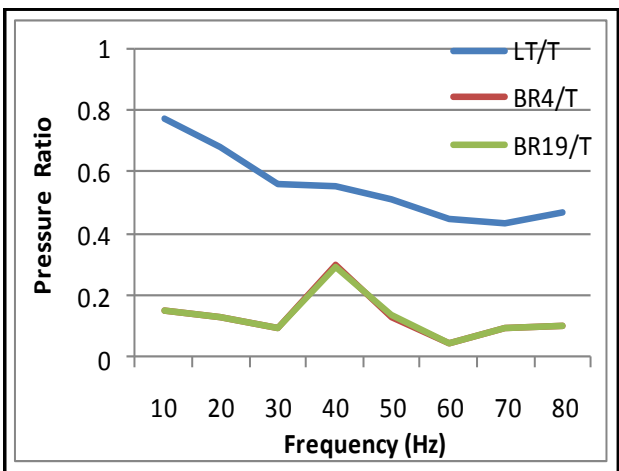
5.2.4 Bronchioles #13 and #28

Figure 5.4 shows the pressure ratio analysis of the Lower Trachea (LT), Bronchi #13 and Bronchi #28 against Trachea (T). In this figure, increasing the respiratory rate shows an increase in the frequency amplitude at Bronchi and Lower Trachea at frequencies between 30Hz and 50Hz. Frequency power at Lower Trachea shows a slight increase with the increasing the airflow amplitude. There was distinct and strong spikes observed at the Bronchi around 30Hz at 0.5L/sec respiratory rate and 1V airflow amplitude.



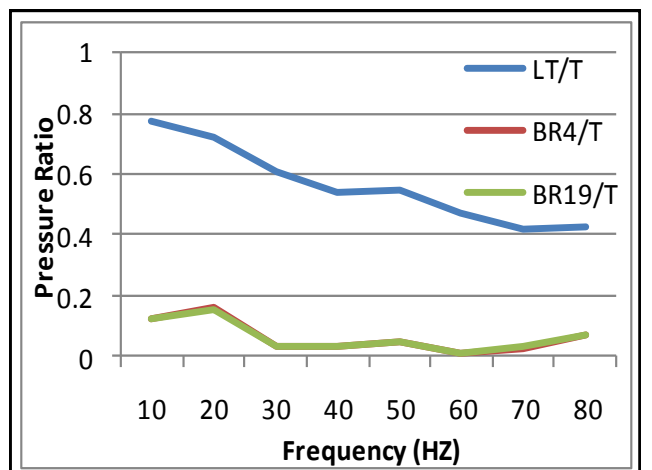
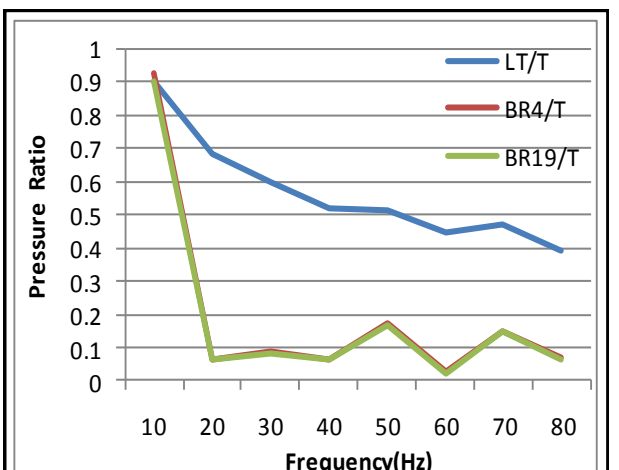
0.5V Airflow Amp. and 0.5b/sec Respiratory rate

1V Airflow Amp. and 0.5b/sec Respiratory rate



0.5V Airflow Amp and 0.55b/sec Respiratory rate

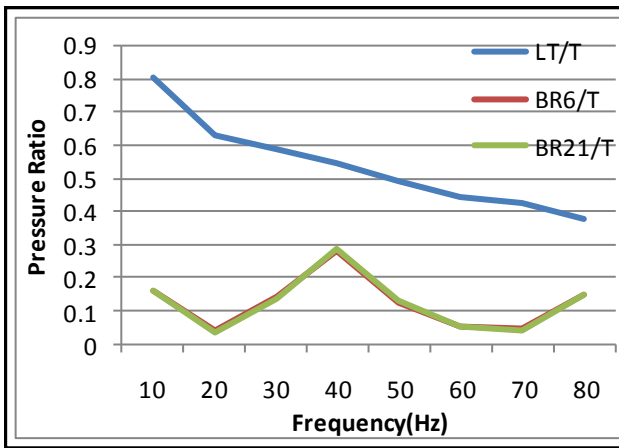
1V Airflow Amp and 0.55b/sec Respiratory rate



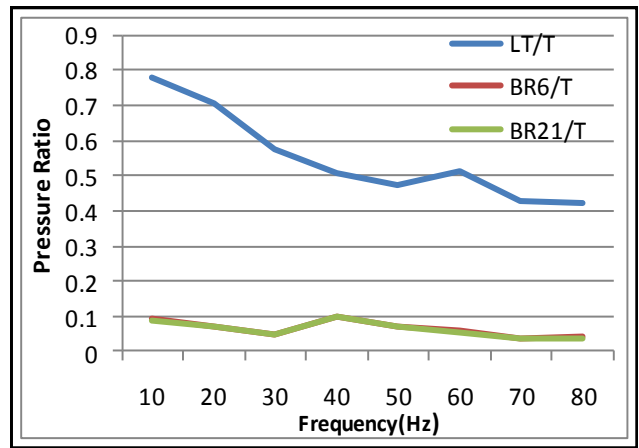
0.5V Airflow Amp and 0.67b/sec Respiratory rate

1V Airflow Amp and 0.67b/sec Respiratory rate

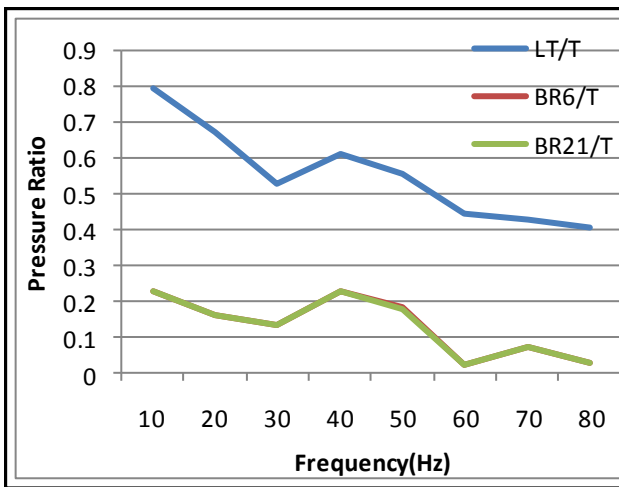
Figure 5.1 -Frequency spectrum of Lower Trachea (LT), Bronchioles (BR) #4 and #19 against Trachea (T)



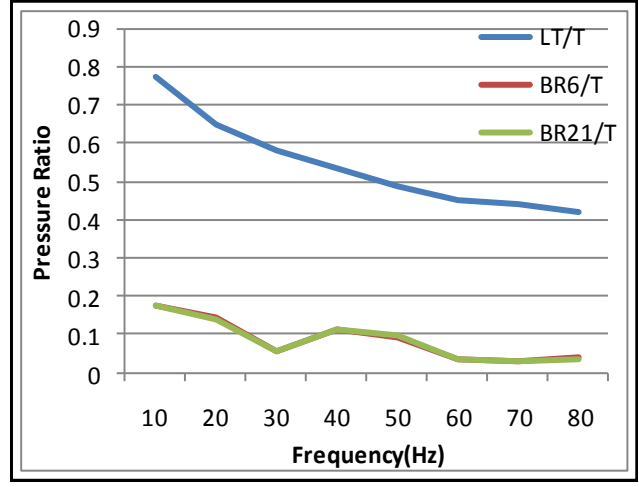
0.5V Airflow Amp. and 0.5b/sec Respiratory



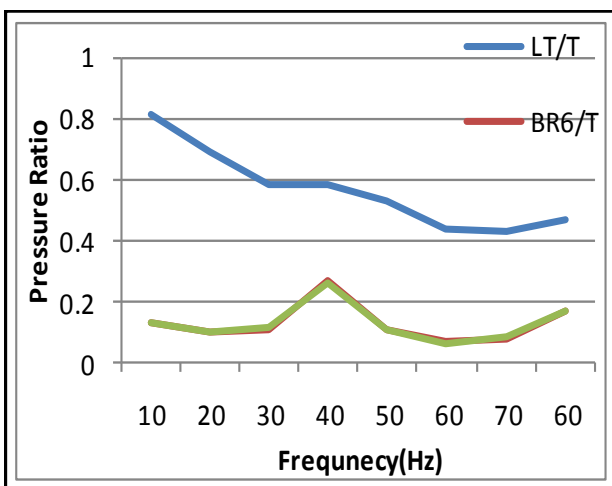
1V Airflow Amp. and 0.5b/sec Respiratory rate



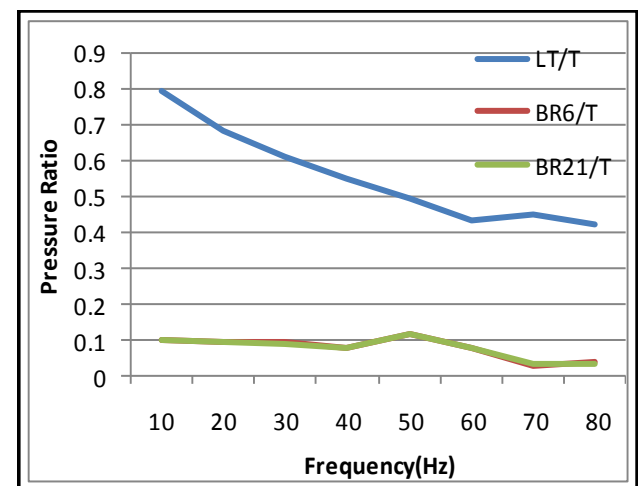
0.5V Airflow Amp. and 0.55b/sec Respiratory



1V Airflow Amp. and 0.55b/sec Respiratory rate

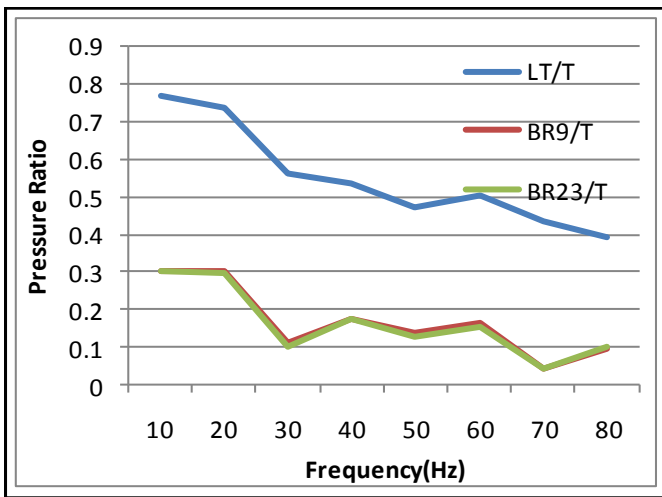


0.5V Airflow Amp. and 0.67b/sec Respiratory

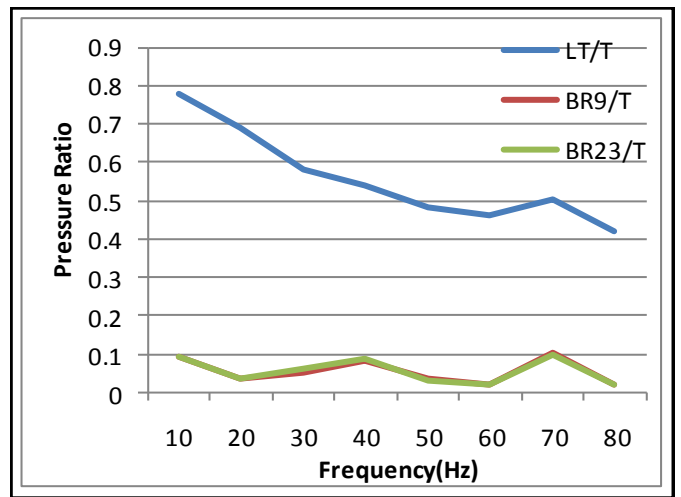


1V Airflow Amp. and 0.67b/sec Respiratory

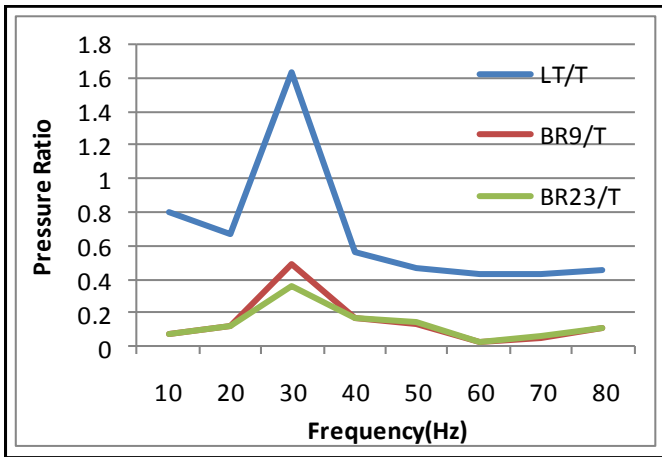
Figure 5.2 -Frequency spectrum of Lower Trachea (LT), Bronchioles (BR) #6 and #21 against Trachea (T)



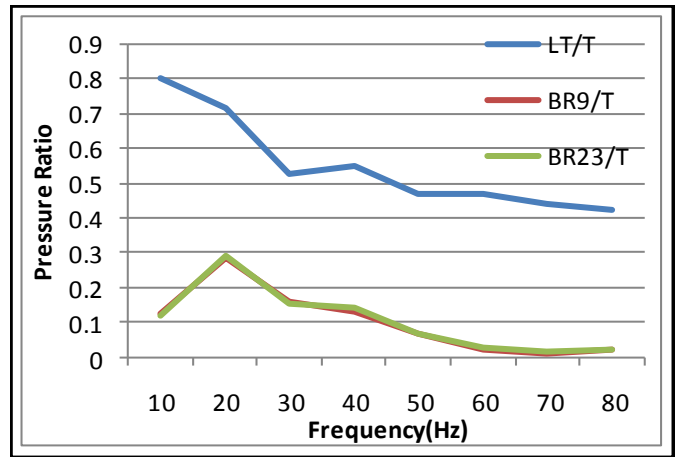
0.5V Airflow Amp & 0.5b/sec Respiratory rate



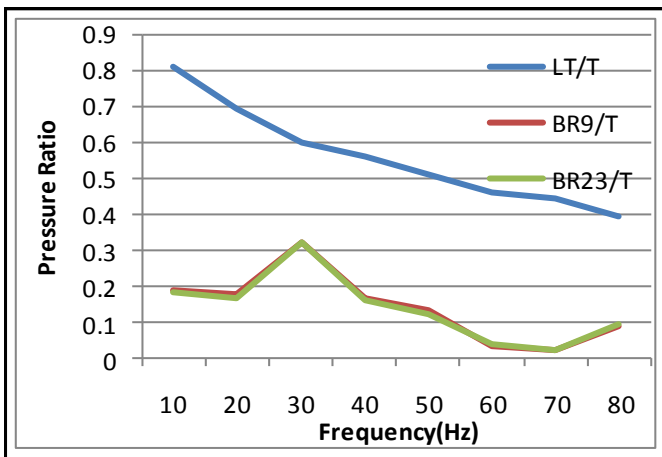
1V Airflow Amp & 0.5b/sec Respiratory rate



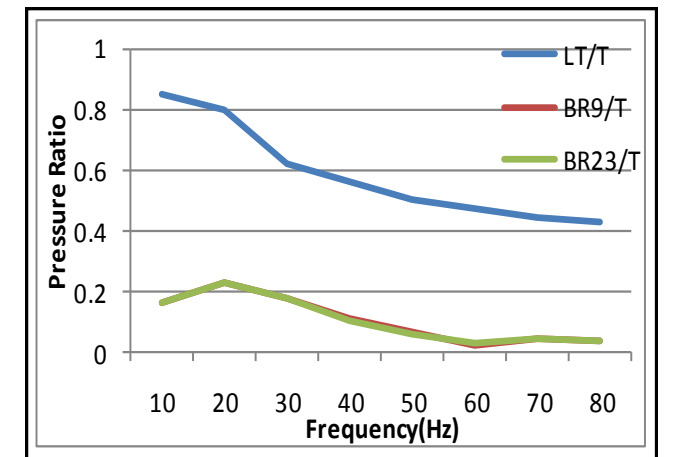
0.5V Airflow Amp & 0.55b/sec Respiratory rate



1V Airflow Amp & 0.55b/sec Respiratory rate

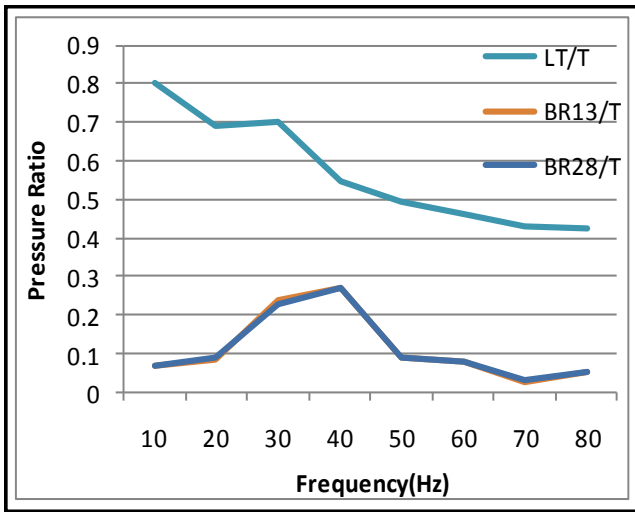


0.5V Airflow Amp & 0.67b/sec Respiratory rate

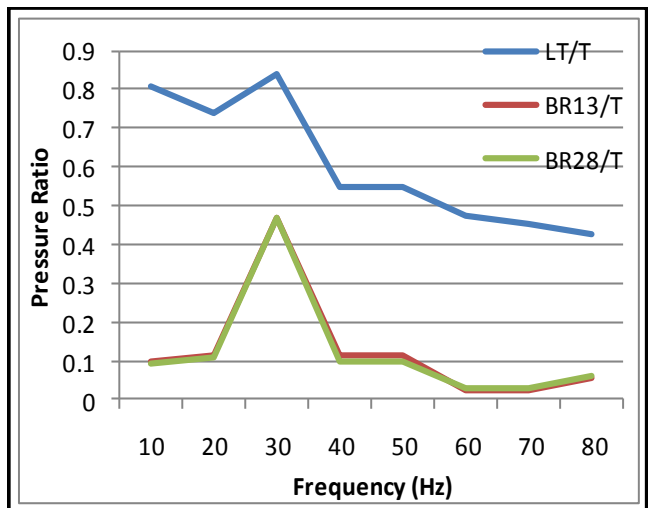


1V Airflow Amp & 0.67b/sec Respiratory rate

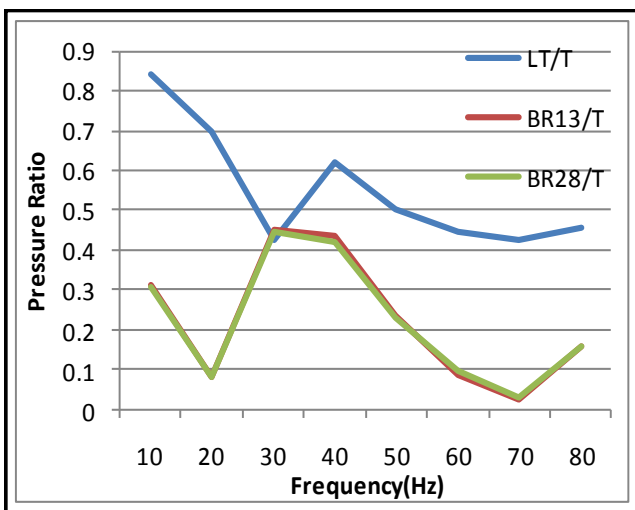
Figure 5.3 -Frequency spectrum of Lower Trachea (LT), Bronchioles (BR) #9 and #23 against Trachea (T)



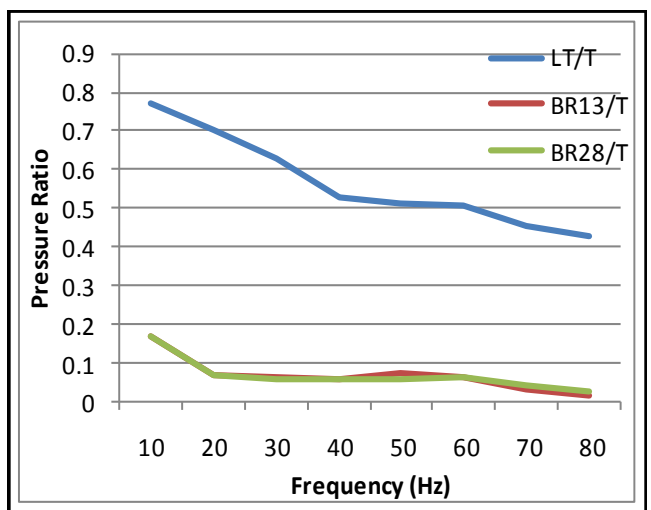
0.5V Airflow Amp & 0.5b/sec Respiratory rate



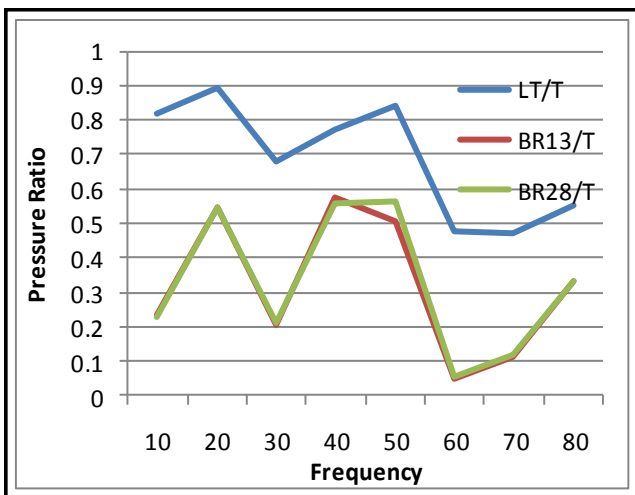
1V Airflow Amp & 0.5b/sec Respiratory rate



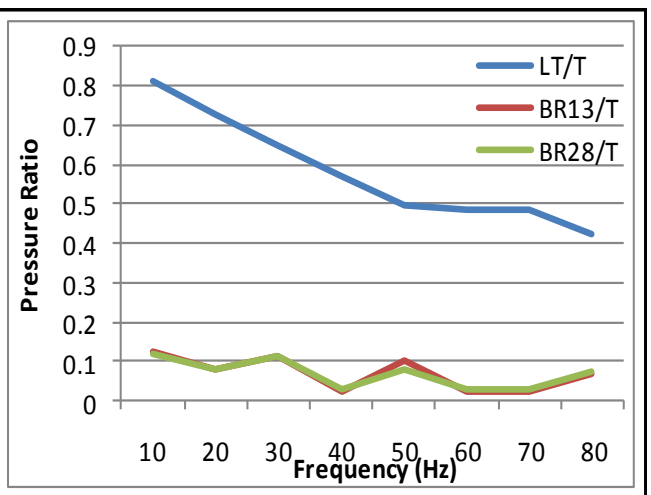
0.5V Airflow Amp & 0.55b/sec Respiratory rate



1V Airflow Amp & 0.55b/sec Respiratory rate



0.5V Airflow Amp & 0.67b/sec Respiratory rate



1V Airflow Amp & 0.67b/sec Respiratory rate

Figure 5.4 -Frequency spectrum of Lower Trachea (LT), Bronchioles (BR) #13 and #28 against Trachea (T)

5.3 Airway Test on 128 day lung casts

This section includes the test result from the 128 day gestation lamb airway tree cast. The test process done as outlined on the test procedure using the different combination lung volume and airflow amplitude as listed on Table 3.2.

5.3.1 Bronchi #3 and #16

Increasing the airflow amplitude showed a decrease in oscillation power at the bronchi as seen in Figure 5.5. When the respiratory rate increased, low power (0.2-0.3) was observed at the Bronchi at frequencies of 30Hz, 50Hz and 70Hz. Increasing the airflow amplitude didn't show any significant change in oscillation power at the Lower Trachea. At 0.67L/sec respiratory rate, there was a very distinct and strong spike (0.7-0.8) at 60Hz. Increasing the respiratory rate shows a slight increase in the oscillation amplitude at Bronchi across all the frequencies.

5.3.2 Bronchi #12and #27

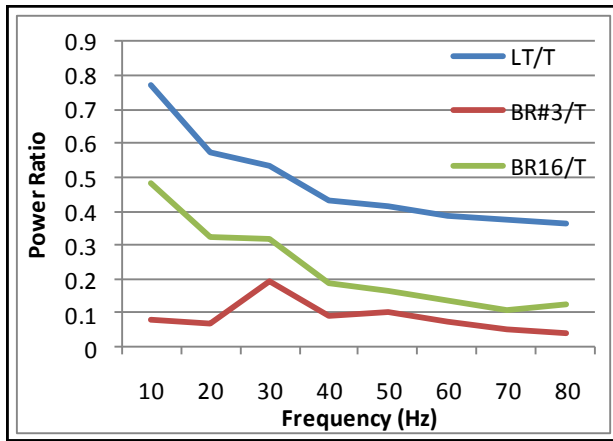
The pressure ratio analysis of the Lower Trachea (LT), Bronchi #12 and Bronchi #27 against Trachea (T), Figure 5.6, shows a slight increase in the oscillation power at the Bronchi and Lower Trachea at 30Hz and 60Hz when the airflow amplitude increased. A strong power (0.8-0.9) is observed around 60Hz at 0.67L/sec respiratory rate. A distinct and strong spike noticed at the Lower Trachea and Bronchi around 60Hz.

5.3.3 Bronchi #4 and #25

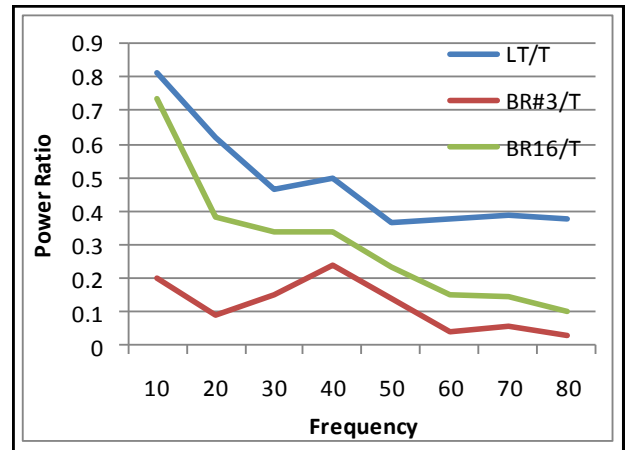
Figure 5.7 shows the pressure ratio analysis of the Lower Trachea (LT), Bronchi #4 and #25 against Trachea (T). At 0.55L/sec respiratory rate, there was a distinct and strong spike (0.7-0.8) noticed at 20Hz as seen in Figure 4.6. There is a distinct spike noticed at the Bronchi around 60Hz with the airflow amplitude of 0.55V. Increasing the airflow amplitude showed a slight decrease in oscillation power at Lower Trachea and Bronchi at 0.5L/sec and 0.67L/sec respiratory rate.

5.3.4 Bronchi #14 and #23

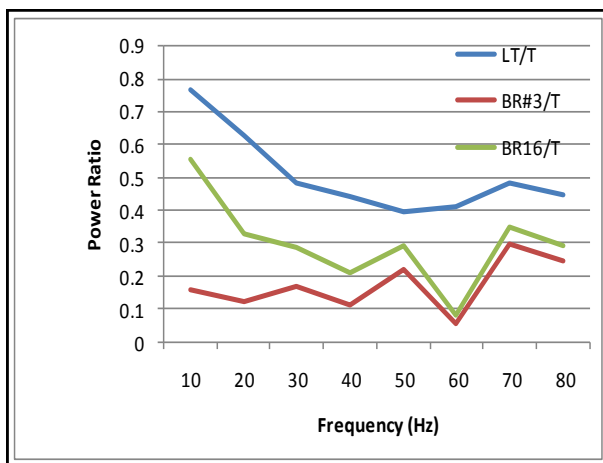
Figure 5.8 shows the pressure ratio analysis of the Lower Trachea (LT), Bronchi #14 and #23 against Trachea (T). No significant change in oscillation amplitude at the Lower Trachea across all frequency range shown in this figure. At 0.67L/sec respiratory rate, increasing the airflow amplitude showed a slight increase in the oscillation power at Bronchi at 20Hz and 40Hz. Spike with moderate amplitude of 0.55 appeared at Bronchi at 50Hz, when the respiratory rate increased to 0.67L/sec.



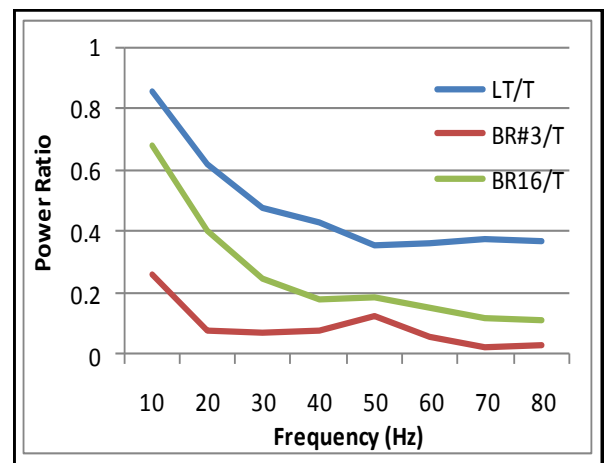
0.5V Airflow Amp & 0.5b/sec Respiratory rate



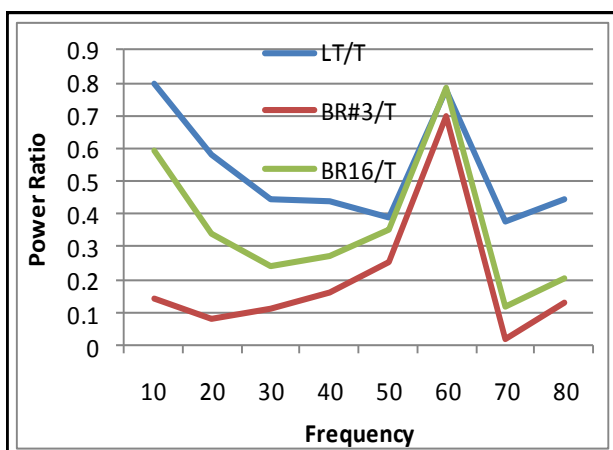
1V Airflow Amp & 0.5b/sec Respiratory rate



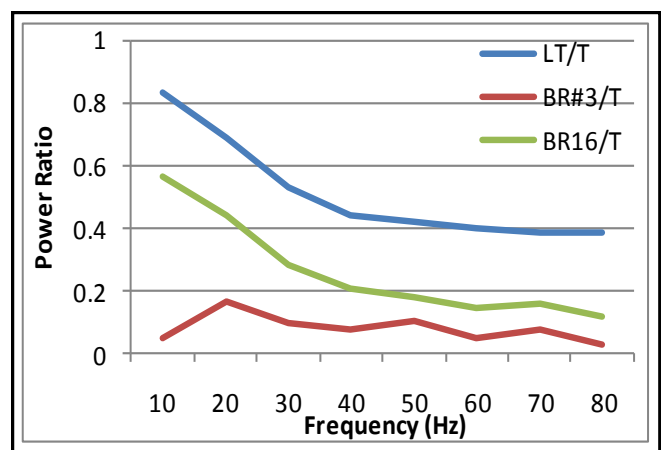
0.5V Airflow Amp & 0.55b/sec Respiratory rate



1V Airflow Amp & 0.55b/sec Respiratory rate

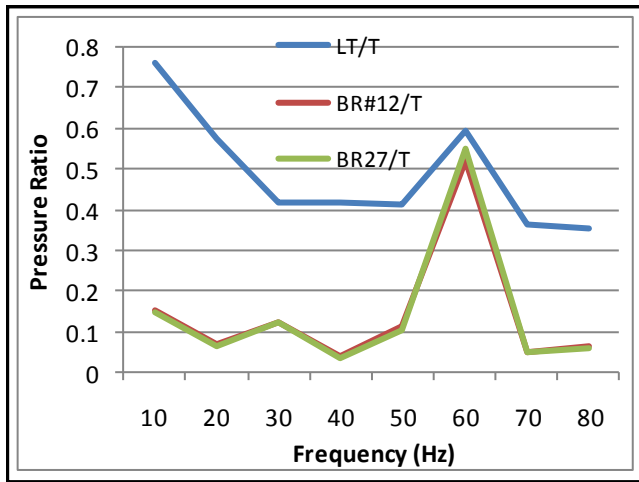


0.5V Airflow Amp & 0.67b/sec Respiratory rate

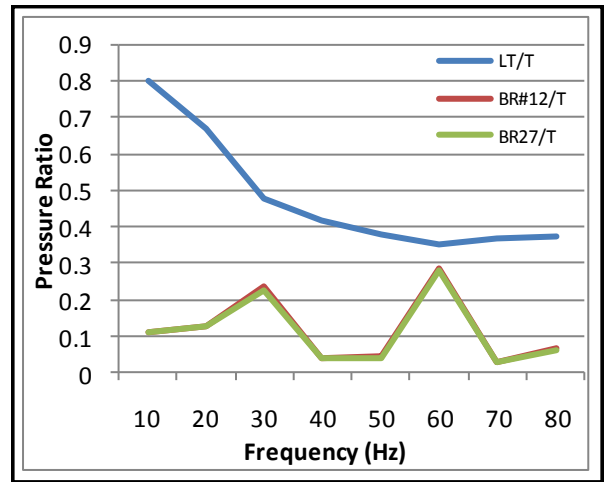


1V Airflow Amp & 0.67b/sec Respiratory rate

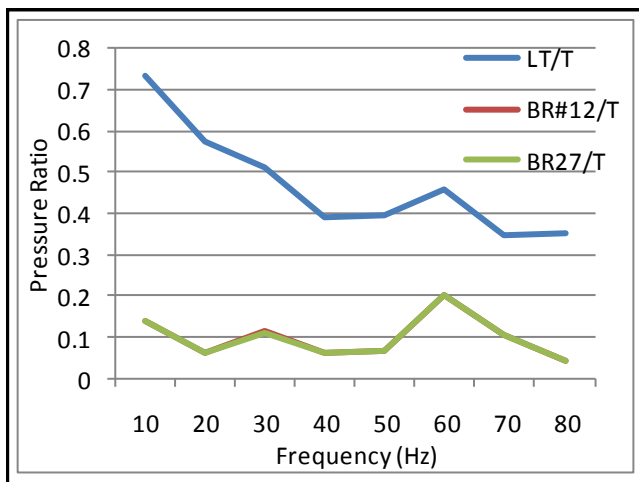
Figure 5.5 - Frequency spectrum of Lower Trachea (LT), Bronchioles (BR) #3 and #16 against Trachea (T)



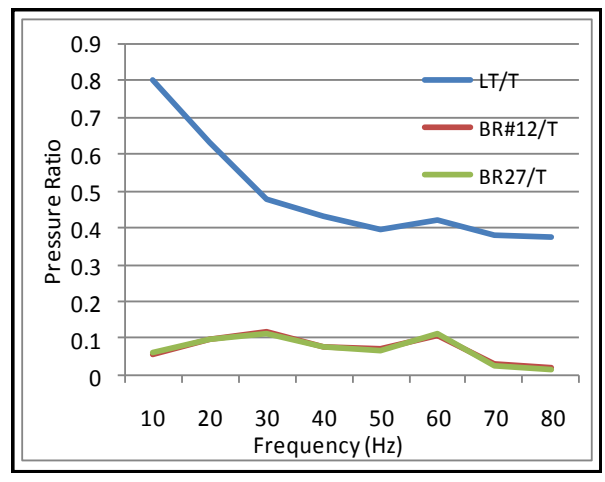
0.5V Airflow Amp & 0.5b/sec Respiratory rate



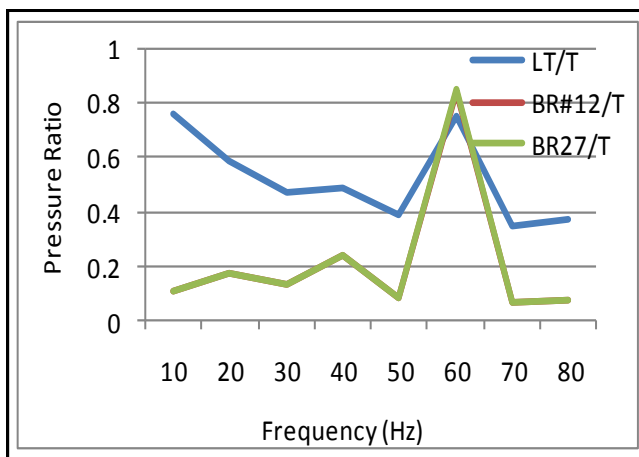
1V Airflow Amp & 0.5b/sec Respiratory rate



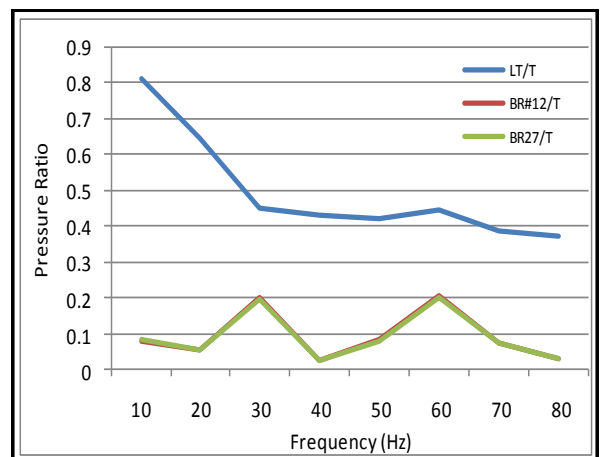
0.5V Airflow Amp & 0.55b/sec Respiratory rate



1V Airflow Amp & 0.55b/sec Respiratory rate

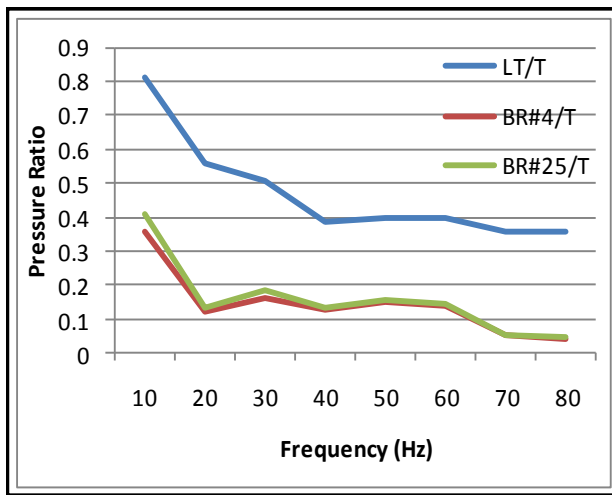


0.5V Airflow Amp & 0.67b/sec Respiratory rate

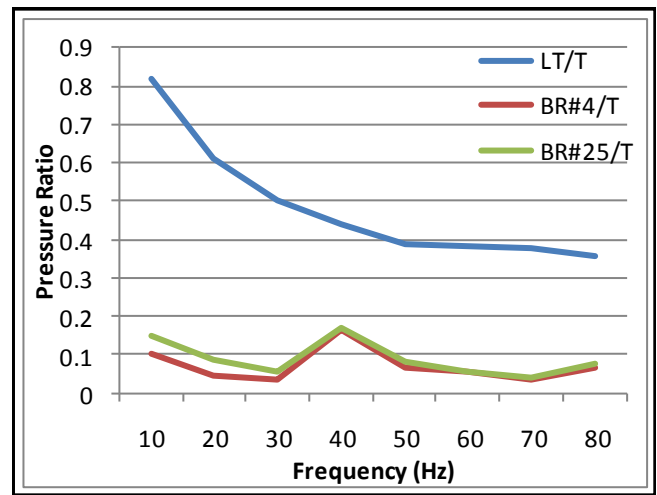


1V Airflow Amp & 0.67b/sec Respiratory rate

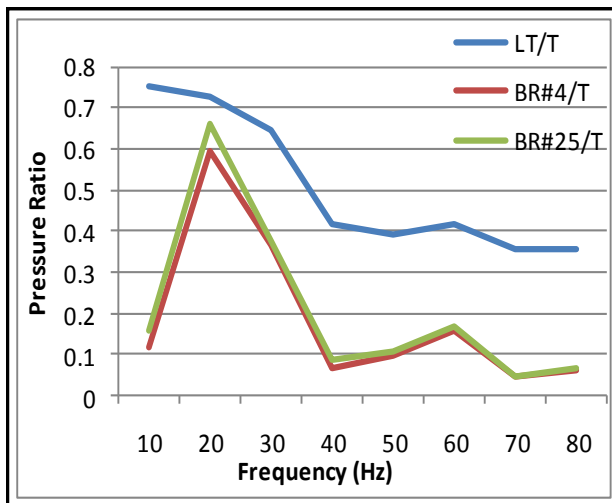
Figure 5.6 -Frequency spectrum of Lower Trachea (LT), Bronchioles (BR) #12 and #27 against Trachea (T)



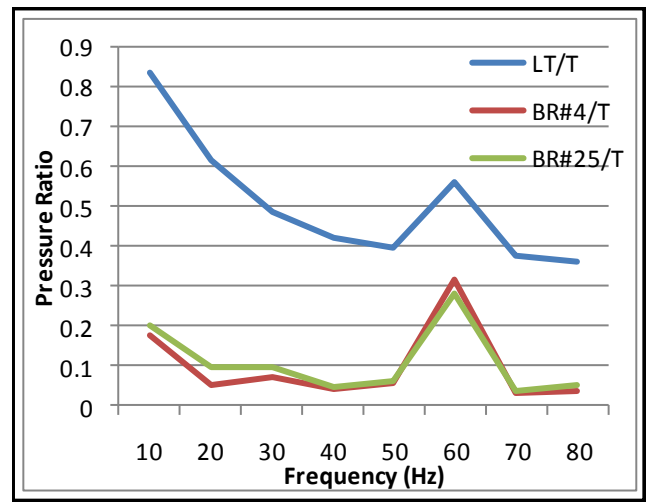
0.5V Airflow Amp & 0.5b/sec Respiratory rate



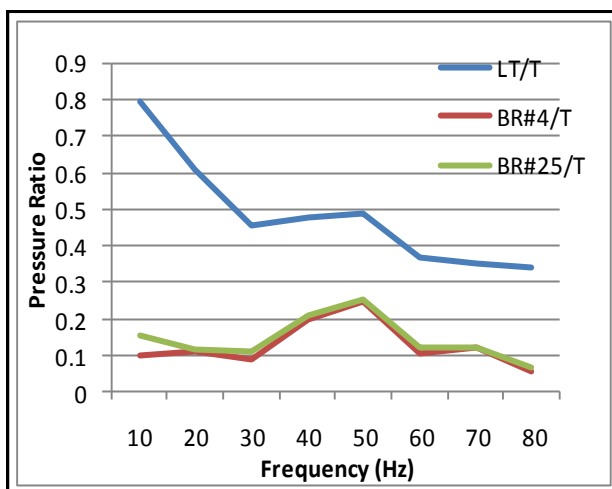
1V Airflow Amp & 0.5b/sec Respiratory rate



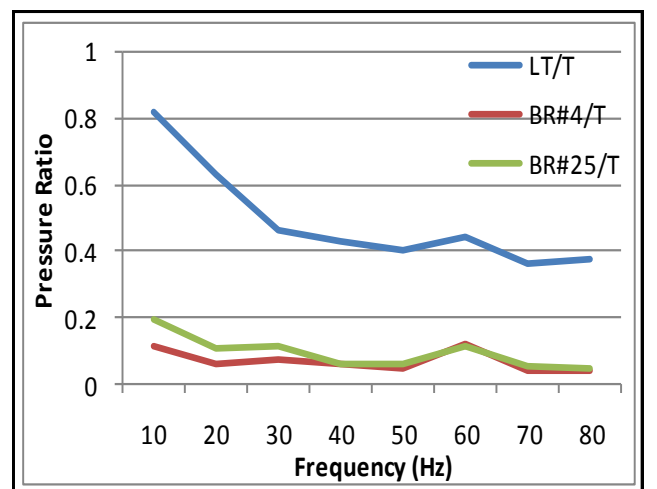
0.5V Airflow Amp & 0.55b/sec Respiratory rate



1V Airflow Amp & 0.55b/sec Respiratory rate

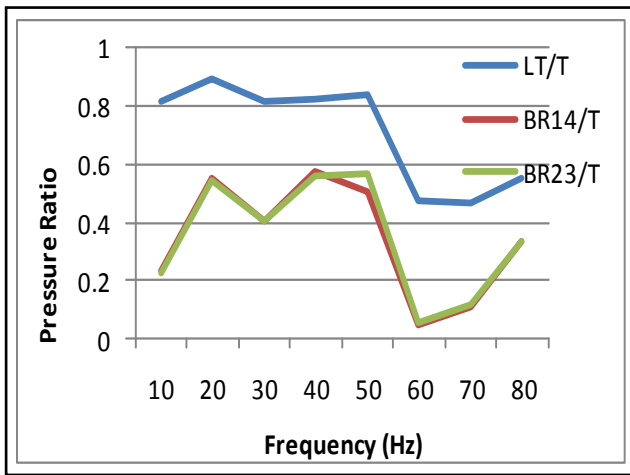


0.5V Airflow Amp & 0.67b/sec Respiratory rate

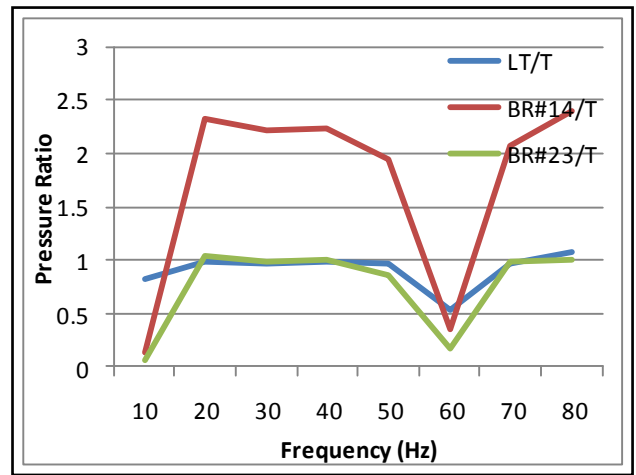


1V Airflow Amp & 0.67b/sec Respiratory rate

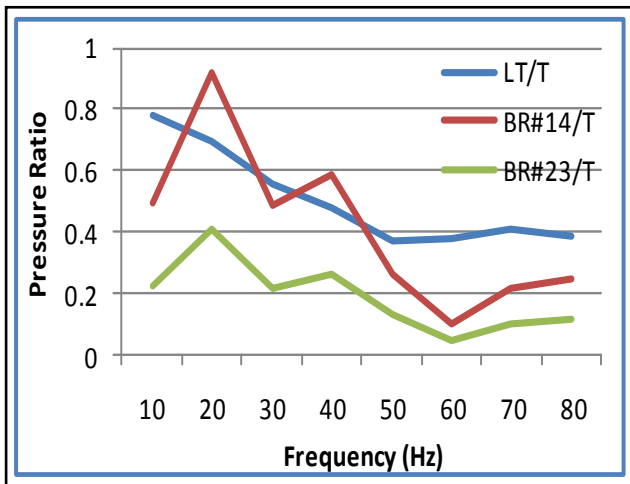
Figure 5.7 -Frequency spectrum of Lower Trachea (LT), Bronchioles (BR) #4 and #25 against Trachea (T)



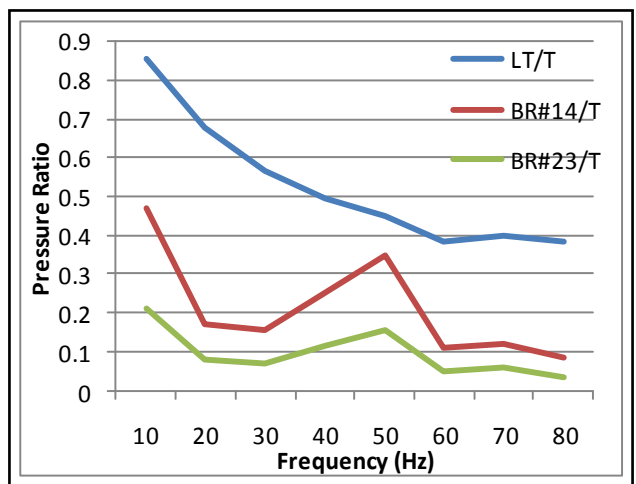
0.5V Airflow Amp. and 0.5L/min Lung volume



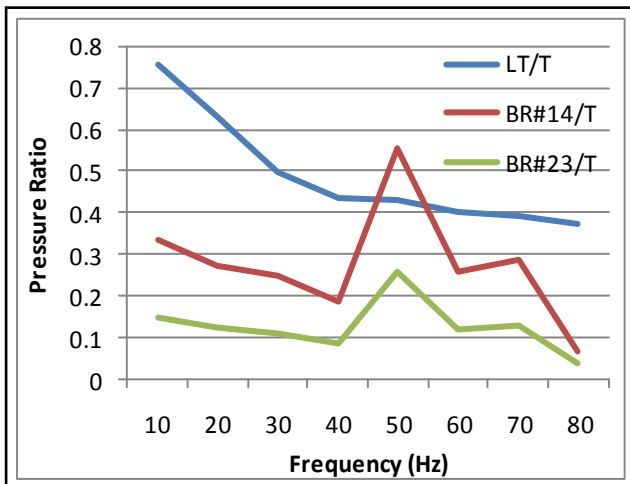
1V Airflow Amp. and 0.5L/min Lung volume



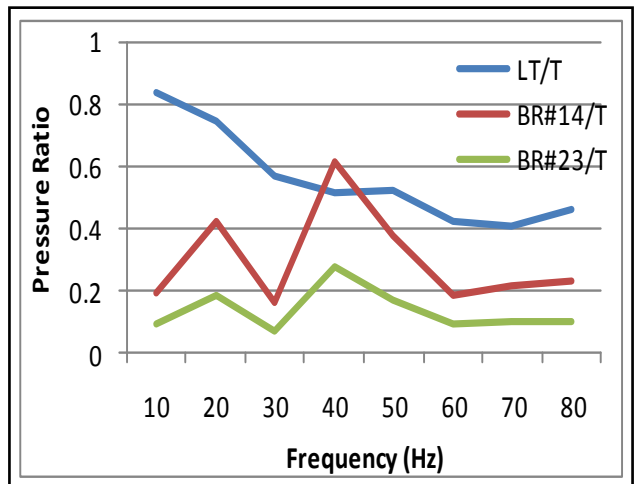
0.5V Airflow Amp. and 0.55L/min Lung volume



1V Airflow Amp. and 0.55L/min Lung volume



0.5V Airflow Amp. and 0.67L/min Lung volume



1V Airflow Amp. and 0.67L/min Lung volume

Figure 5.8 -Frequency spectrum of Lower Trachea (LT), Bronchioles (BR) #14 and #23 against Trachea (T)

5.4 Modelling Result

Model analysis helps to compare and validate the experimental result. This modeling result compares the pressure oscillation value between the casted lung and the computer model. The pressure value measured at the trachea during the experimental testing used as an input value for the modeling system. Which intends to make the input values same. Pressure ratio calculated by dividing each airway pressure value by the trachea pressure value.

The following figures show the test result from the 142 day gestation lamb model using different respiratory rates. Figure 5.9 to Figure 5.11 show the frequencies of pressure oscillations and their magnitude for each particular airway.

Increasing the respiratory rate shows an overall increase in the oscillation amplitude at all airways across all the frequencies. A moderate spike was observed to appear at 40Hz and 60Hz at 0.5b/sec respiratory rate as well as at 20Hz at 0.55b/sec respiratory rate.

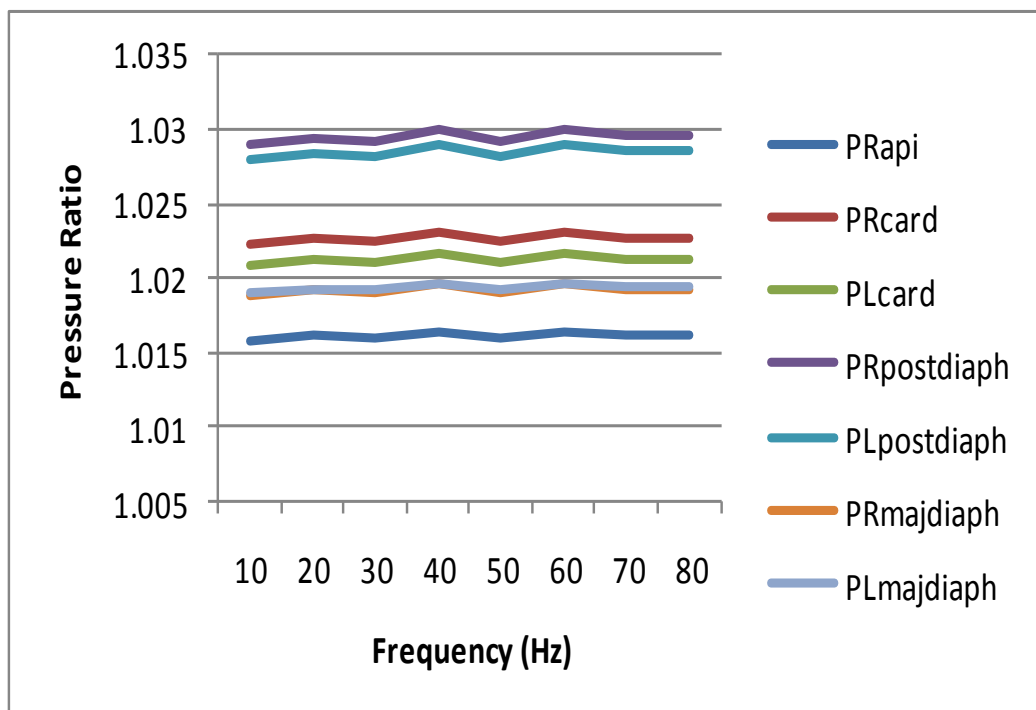


Figure 5.9 Frequency Spectrum of airways at 0.5b/sec respiratory rate

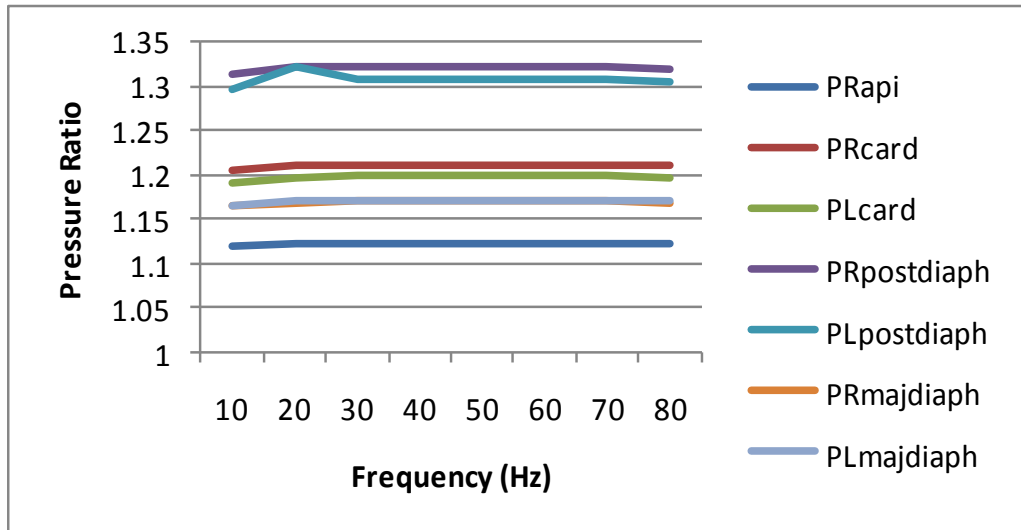


Figure 5.10 Frequency Spectrum of airways at 0.55b/sec respiratory rate

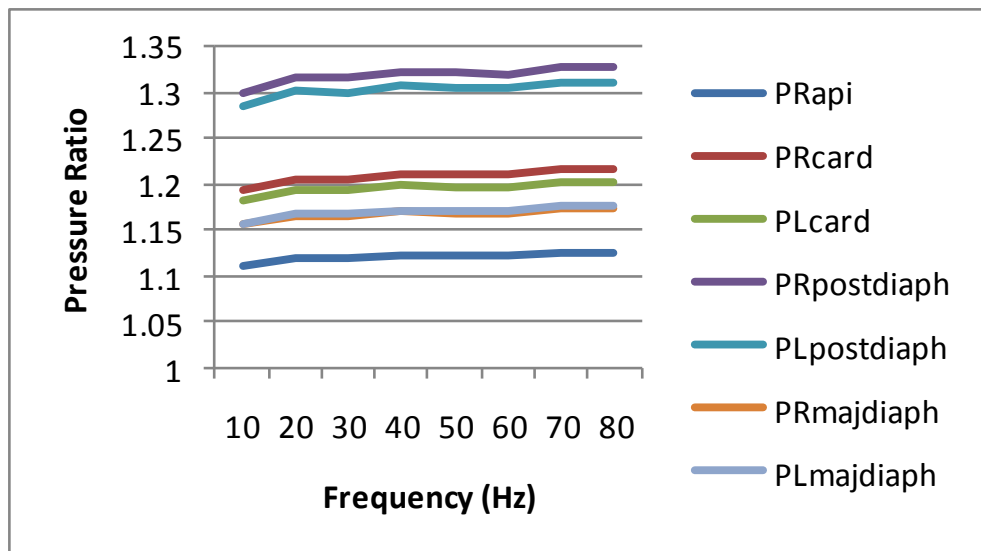


Figure 5.11 Frequency Spectrum of airways at 0.67b/sec respiratory rate

The pressure in the right post diaphragmatic airway and the right cardiac airway were slightly greater than the left diaphragmatic airway and left cardiac airway respectively. The left cardiac airway shows larger magnitude of pressure than the left apical airway. Similarly the right cardiac airway shows larger magnitude of pressure than the right apical airway. The left major diaphragmatic airway and the right major diaphragmatic airway shows similar magnitude of pressure to each other. In general the right side airways (which are slightly bigger than the left airways) show a slightly greater pressure value than the left side airways.

CHAPTER 6

DISCUSSION

6.1. Introduction

This chapter discusses the casting process as well as the experimental and modeling results. Section 6.2 starts by discussing the identified casting process of making a lung cast. Experimental results of looking at the transmission of the respiratory rate and frequency amplitude to bronchi are discussed in section 6.3. Section 6.4 discusses the results of the modeling analysis presented in Chapter 5. The experimental results are compared with model predictions and discussed.

6.2 Enhanced Casting Process

An investigation on manufacturing a hollow airway cast was performed in Chapter 2. This study identified a simple, fast and reasonably cost effective process of making an airway cast. The following is a discussion of the results of making hollow airway cast.

Even though several methods have been attempted [25, 38, 48, 49] to produce a hollow airway casts before, the methods used in these works have disadvantages in a number of ways. To cite a few, using wax at the first stage of making a negative cast reduces the airway size because of shrinkage upon cooling while going down in wet lung. Wood's metal needs a dried lung which delays the process by several days and also controlling its temperature up on pouring is a challenge. However, we found that silicone was the best option as it doesn't need a dried lung as well as has minimal shrinkage.

The biggest challenge in this process was achieving an evenly painted negative cast. Even though dipping or spraying are other alternatives, smaller airway branches can be broken easily during the dipping process as well as banana-skin silicone is not manufactured as a spray material. The final option was to paint the negative cast with several times in equal interval to keep the airway thickness even. In conclusion, we have found this process relatively simple for production of practically accurate airways. We believe these casts provide a useful model to investigate how far the pressure oscillation frequencies can travel the airways.

6.3 Experimental Result

To further study the results in terms of the effect of the reparatory rate, the highest pressure ratio value of all bronchioles was studied. Figure 6.1 and Figure 6.2 shows the summary of the highest pressure ratio value at each Bronchiole for each particular breathing rate. Figures 6.3 and Figure 6.4 illustrate the highest frequency of pressure oscillations measured at different bronchiole locations of 142g lamb cast and 128g lamb cast respectively.

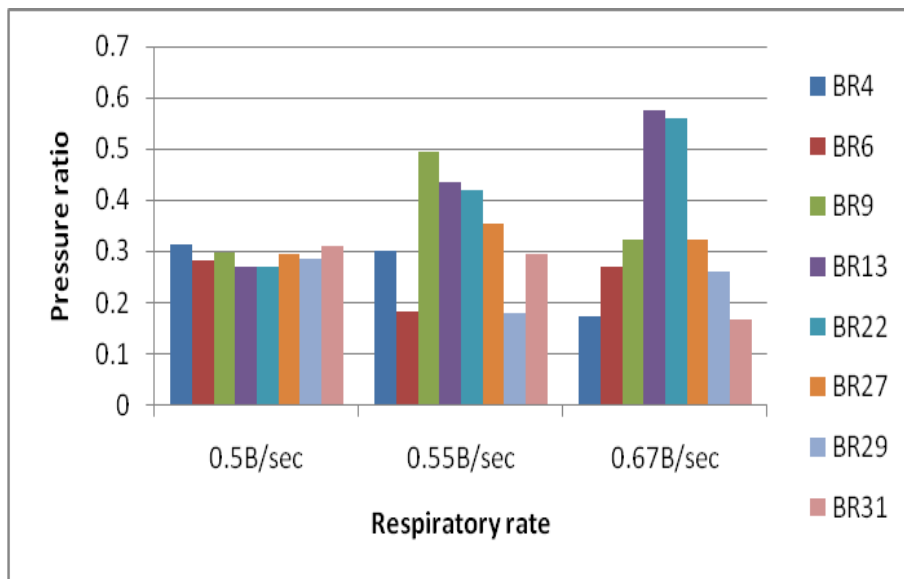


Figure 6.1 – Highest amplitude of each Bronchiole at particular breathing rate, from 142g lamb cast

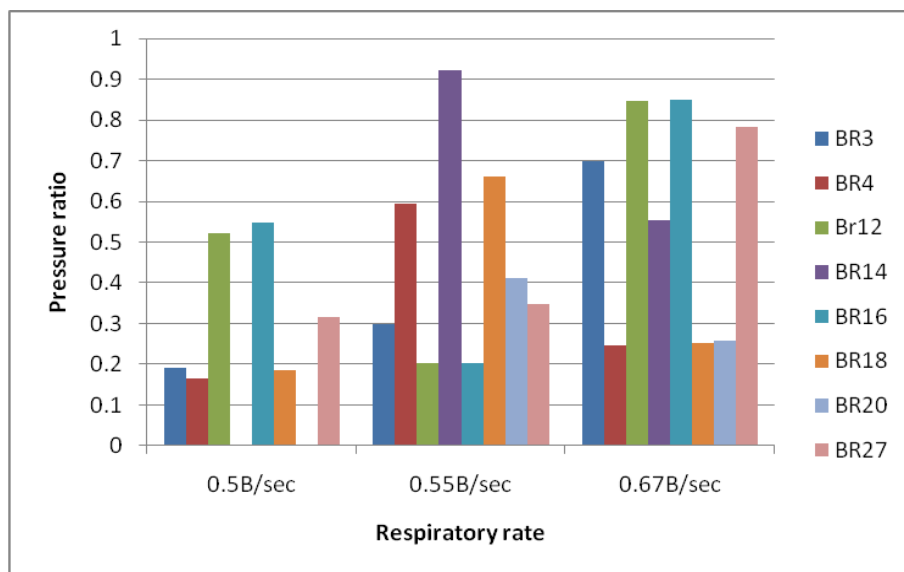


Figure 6.2 – Highest amplitude of each Bronchiole at particular breathing rate, from 128g lamb cast

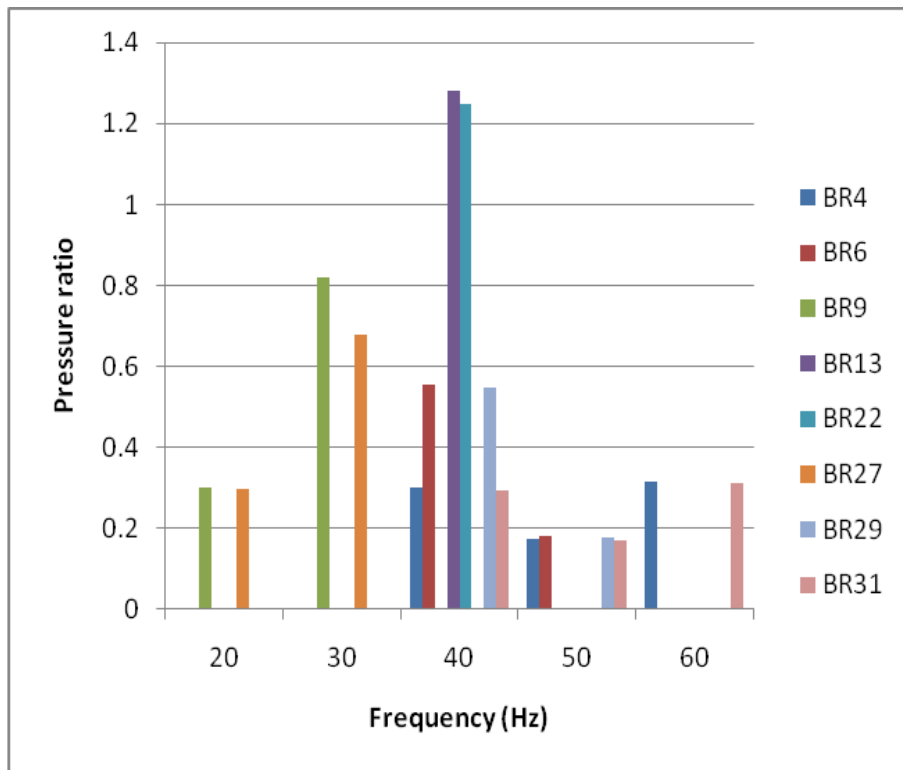


Figure 6.3 – Frequencies with the highest amplitude at each bronchiole, from 142 g lamb cast

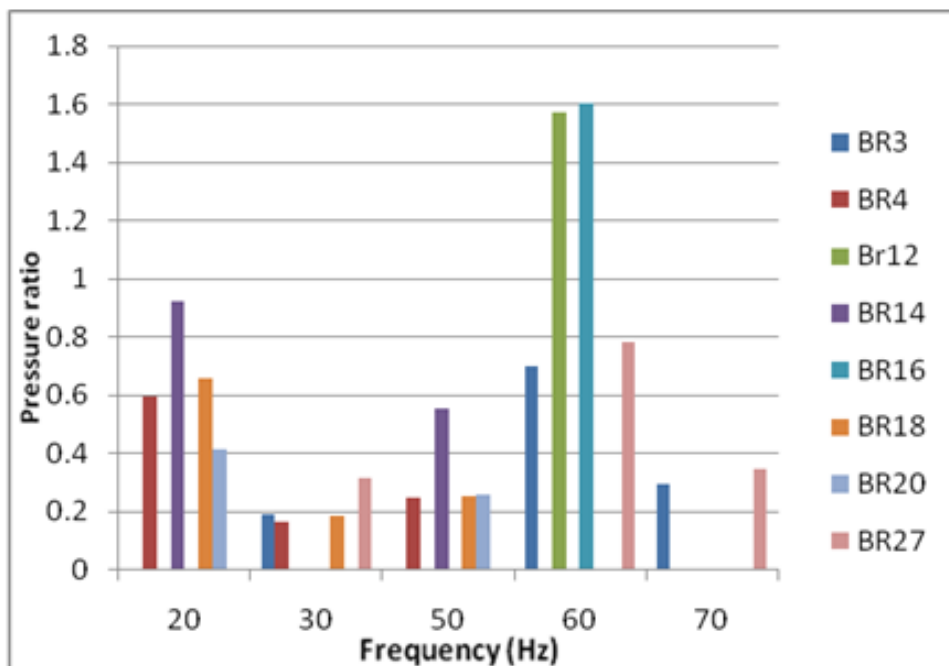


Figure 6.4 – Frequencies with the highest amplitude at each bronchiole, from 128 g lamb cast

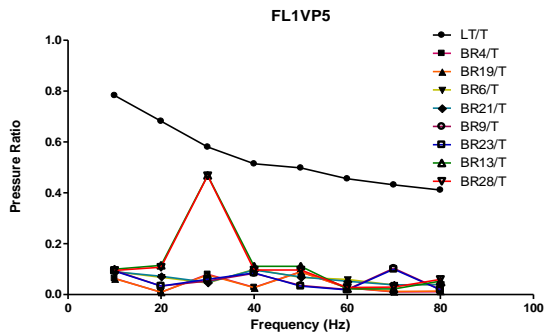
In terms of the respiratory rate, the 142 day gestation lamb showed similar pressure oscillation amplitudes across all the bronchi at 0.5b/sec respiratory rate. Increasing the respiratory rate shows an overall decrease in the pressure oscillation amplitude at Lower Trachea and Bronchi. Even though some Bronchi (#13 and #22) appeared to have spikes with high amplitude as the respiratory rate increases, 0.5b/sec was the optimal respiratory rate for 142 day gestation lamb. It also reported by Pillow [45] that the respiratory rate for 146 day gestation lambs is approximately 30 breaths per minute (bpm) which is 0.5b/sec. Increasing airflow amplitude showed a decrease in the pressure oscillation amplitude at the bronchi. There were distinct and strong spikes noticed at the Bronchi around 30Hz and 40Hz, for 0.5v airflow amplitude.

It is also noted that 128 day gestation lamb showed similar pressure oscillation amplitude across most of the bronchi at 0.67b/sec respiratory rate. Similarly it is report by Pillow [45] that the respiratory rate for 125 day and 135 day gestation lambs is 40 breaths per minute (bpm) which is 0.67b/sec. Hence we can say that it is the most favorable respiratory rate for 128 day gestation lamb. Increasing the airflow amplitude showed a decrease in pressure oscillation amplitude at Bronchi while didn't show any significant change at the Lower Trachea. When the respiratory rate increased to 0.67L/sec, a strong power (0.8-0.9) observed around 20Hz.

Previous research [50] proposed that these strong pressure oscillation frequencies (around 30Hz) have beneficial contribution to the lung recruitment and relaxation. In particular the preterm neonatal lung resonant frequency have been measured around 29Hz [51]. Thus it indicates a possibility of delivering a particular pressure oscillation frequency that match the resonant frequency of a particular neonatal.

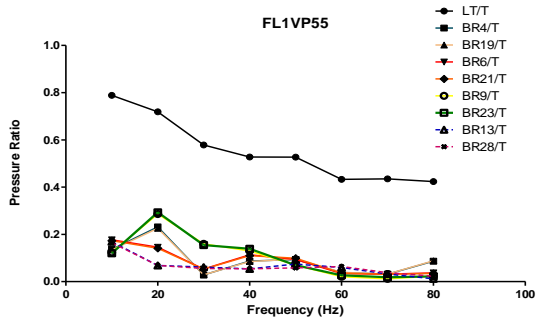
6.4 Statistical Analysis

This section lists the statistical analysis result which is performed in order to assess the experimental result. Figure 6.5 and Figure 6.6 shows the statistical analysis result from the 142day and 128day gestation lamb respectively. Based on the one way ANOVA analysis result below in the tables, the mean difference between the inlet (Trachea) pressure ratio value and the outlet (Bronchi) pressure ratio value is large enough to be considered as shown by P value.



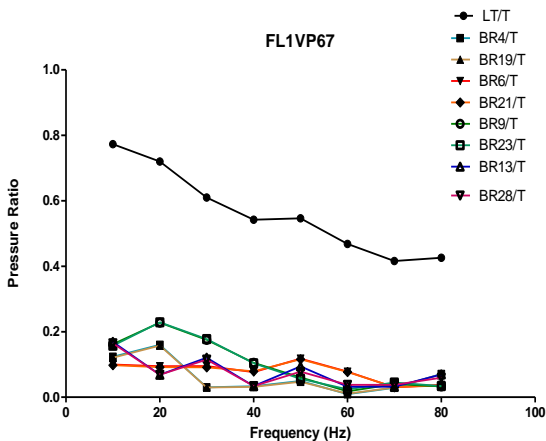
One-way analysis of variance	
P value	< 0.0001
P value summary	****
Are means signif. different? (P < 0.05)	Yes
Number of groups	9
F	29.42
R square	0.7889

1V Airflow Amp. and 0.5b/sec Respiratory rate



One-way analysis of variance	
P value	< 0.0001
P value summary	****
Are means signif. different? (P < 0.05)	Yes
Number of groups	9
F	32.07
R square	0.8029

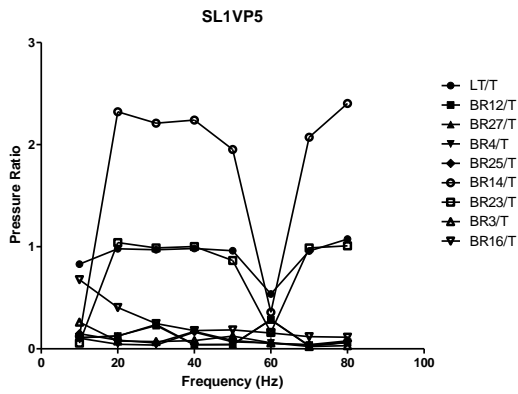
1V Airflow Amp. and 0.55b/sec Respiratory rate



One-way analysis of variance	
P value	< 0.0001
P value summary	****
Are means signif. different? (P < 0.05)	Yes
Number of groups	9
F	46.01
R square	0.8539

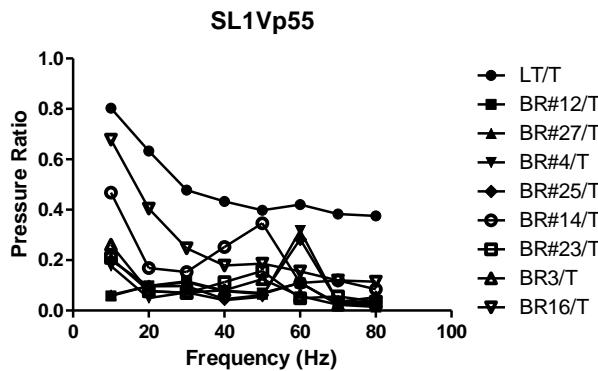
1V Airflow Amp. and 0.67b/sec Respiratory rate

Figure 6.5 Statistical graphs from the 142day gestation lamb experimental result using different respiratory rate values



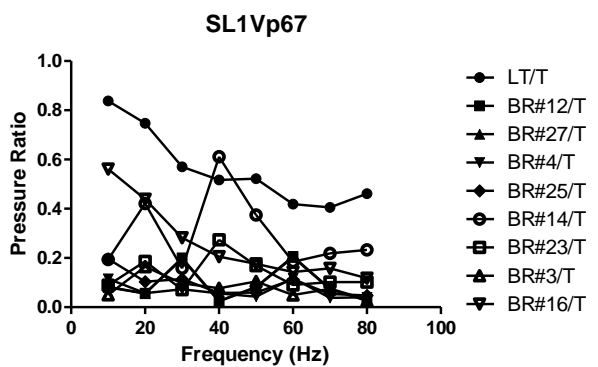
One-way analysis of variance	
P value	< 0.0001
P value summary	****
Are means signif. different? (P < 0.05)	Yes
Number of groups	9
F	20.84
R square	0.7258

1V Airflow Amp. and 0.5b/sec Respiratory rate



One-way analysis of variance	
P value	< 0.0001
P value summary	****
Are means signif. different? (P < 0.05)	Yes
Number of groups	9
F	12.78
R square	0.6188

1V Airflow Amp. and 0.55b/sec Respiratory rate



One-way analysis of variance	
P value	< 0.0001
P value summary	****
Are means signif. different? (P < 0.05)	Yes
Number of groups	9
F	20.19
R square	0.7194

1V Airflow Amp. and 0.67b/sec Respiratory rate

Figure 6.6 Statistical graphs from the 128day gestation lamb experimental result using different respiratory rate values

The test process was done using the different combination respiratory rate. The figures above show the frequency spectrum of pressure oscillations and their magnitude for each particular position at the airway tree.

Figure 6.5 show statistical graphs from the 142day gestation lamb experimental result using different respiratory rate values. Increasing the respiratory rate shows a slight increase in the frequency amplitude across all the Bronchioles. It shows distinct and strong spikes at the Bronchi #13 and #28 around 30Hz with respiratory rate of 0.5V. A moderate spike observed to appear at 20Hz with 0.55b/sec and 0.67b/sec respiratory rate.

Figure 6.6 show statistical graphs from the 128day gestation lamb experimental result using different respiratory rate values. Frequency oscillation amplitude at the Bronchioles observed to increase when the respiratory rate increased to 0.67L/sec. When the respiratory rate increased to 0.55L/sec, spikes with moderate amplitude of 0.6 appeared at 40Hz.

6.5 Modeling result

In this section the effect of the frequencies of pressure oscillations on the airway are investigated in order to determine which frequencies are most beneficial for a particular neonate. Figure 6.7 shows the highest frequency of pressure oscillations measured at each airway. Whereas Figure 6.8 shows the summary of the highest Pressure Ratio values at each particular breathing rate.

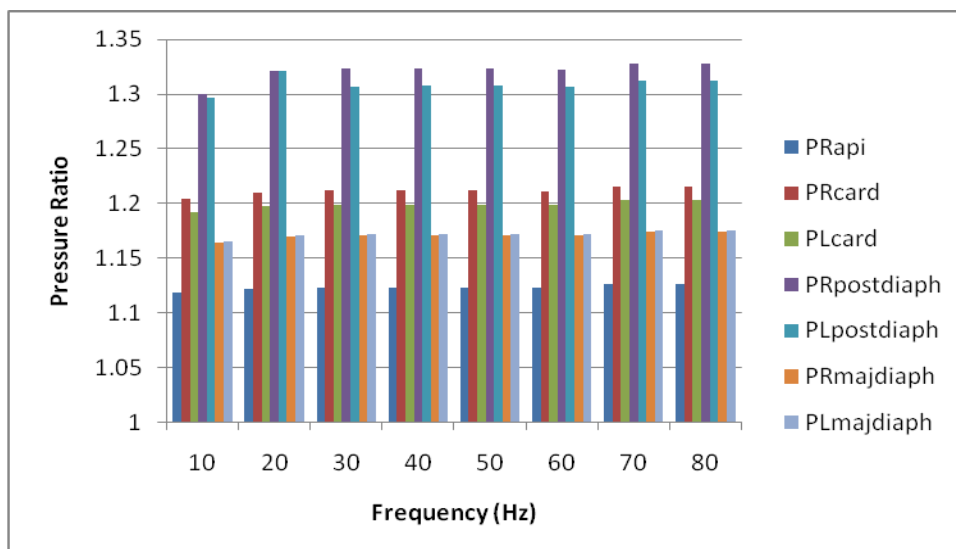


Figure 6.7– Frequencies with the highest amplitude at each airway

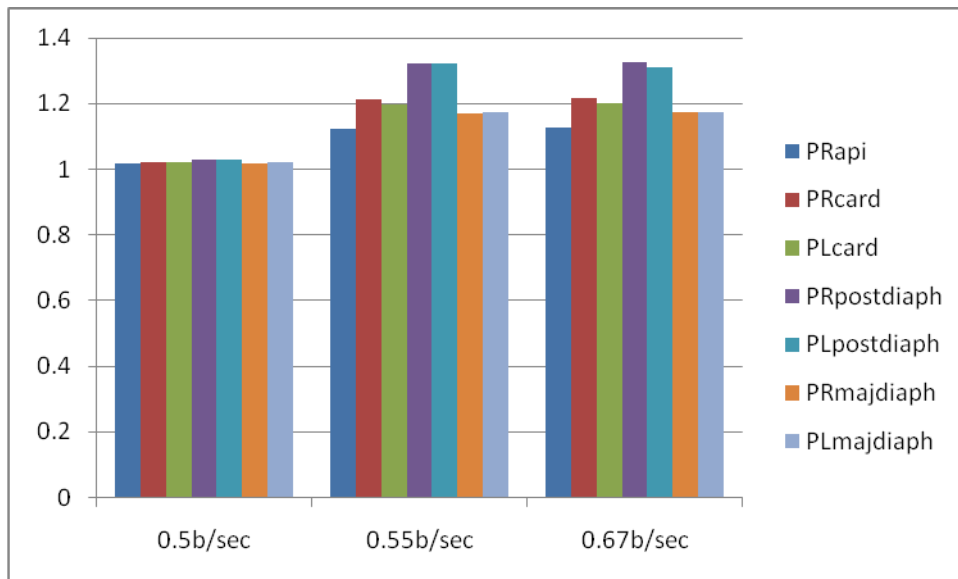


Figure 6.8 Highest amplitude for each airway at a particular breathing rate

In terms of the respiratory rate, all airways showed similar pressure oscillation amplitude across all the branches at lower respiratory rate (0.5b/sec). This correlates with the experimental result. Right posterior diaphragmatic bronchus (Rpostdiaph) and Left posterior diaphragmatic bronchus (Lpostdiaph) appeared to have spikes with high amplitude as the respiratory rate increases. Increasing airflow amplitude showed an overall decrease in the pressure oscillation amplitude on most airway branches, which is similar outcome with the experimental result. All frequencies appeared with highest amplitude at Rpostdiaph and Lpostdiaph.

Figure 6.9 presented the comparison of the experimental values and model predictions. Even though the theoretical modelling used to compare the experimental result was the closest modelling work available, the pressure oscillation amplitudes appeared to be not matching. These can be attributed to the fact that airways modelled as a rigid tube with few stages while the experimental work done closer to the real lung in terms of elasticity, airway stages and angles. In reality airways have some compliance which will reduce the oscillation amplitudes travelling through them. Accurately to determine the mechanical properties of the airways requires detailed experiential measurements which were beyond the scope of this research and remain a subject of further study. The model predictions remain indicative of the transmission of the pressure oscillations at this stage. Table 6.1a and Table 6.1b show pressure value comparison between the experimental and modeling.

Table 6.1a Model Vs Experimental pressure value comparison

	Model	Exp.	Model	Exp.	Model	Exp.	Model	Exp.
Freq.	PRapi	BR4	PRcard	BR6	PLcard	BR19	PRpostdiaph	BR9
10	1.0158	0.0638	1.0222	0.0906	1.0209	0.063	1.029	0.0947
20	1.0161	0.0091	1.0226	0.0682	1.0212	0.0094	1.0293	0.0337
30	1.016	0.08	1.0224	0.0455	1.021	0.0774	1.0292	0.0532
40	1.0164	0.0283	1.023	0.0994	1.0216	0.0272	1.0299	0.0838
50	1.016	0.09	1.0224	0.0677	1.021	0.0889	1.0292	0.0358
60	1.0164	0.0265	1.023	0.0595	1.0216	0.0263	1.03	0.0198
70	1.0162	0.0107	1.0227	0.0376	1.0213	0.012	1.0295	0.1035
80	1.0161	0.011	1.0227	0.0398	1.0213	0.0138	1.0295	0.0199

Table 6.1b Model Vs Experimental pressure value comparison

	Model	Exp.	Model	Exp.	Model	Exp.
Freq.	PLpostdiaph	BR21	PRmajdiaph	BR13	PLmajdiaph	BR28
10	1.028	0.0897	1.0189	0.0995	1.019	0.095
20	1.0284	0.0721	1.0192	0.1146	1.0193	0.1078
30	1.0282	0.048	1.0191	0.4685	1.0192	0.4677
40	1.0289	0.0964	1.0196	0.1114	1.0197	0.0964
50	1.0282	0.0694	1.0191	0.1114	1.0192	0.0964
60	1.029	0.0524	1.0196	0.0228	1.0197	0.028
70	1.0285	0.0381	1.0193	0.0223	1.0194	0.0293
80	1.0285	0.0391	1.0193	0.0531	1.0194	0.0597

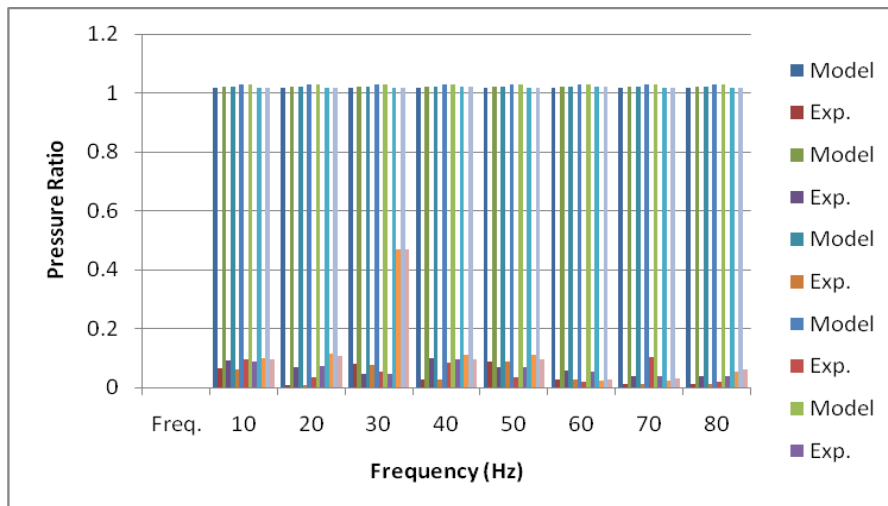


Figure 6. 9 Model Vs Experimental pressure value comparisons

CHAPTER 7

CONCLUSION AND FUTURE WORK

7.1 Conclusion

The objective of this thesis was to establish the effectiveness of Bubble CPAP in transmitting pressure oscillations through the neonatal tracheobronchial tree. As it is almost impossible to perform experimental analysis using human neonatal lung at this stage, the need for developing a lung model was vital to study the effect of pressure oscillations in the neonatal respiratory system. Chapter 2 presented airway casting process. Chapter 3 discussed the experimental investigation to determine how far the pressure oscillation frequencies can travel at the bronchi. Chapter 4 presented the modelling system which is chosen for comparison with experimental data. Results and discussions presented in chapter 5 and chapter 6 respectively.

The following was successfully developed in this research:

- Artificial airway model was made and tested.
- Experimental setup and procedure developed.
- Neonatal Respiratory System Model modified for this work.
- Analyzing the result, spikes of 20Hz, 30Hz and 40Hz frequencies were shown at the level of secondary bronchi with considerable power even though they were relatively low compared to the trachea.

The effect of the respiratory rate and airflow amplitude changes do follow similar trend to the mathematical model predictions. The study indicates that pressure waves with different frequencies can be delivered to different locations of the lung by controlling the pressure oscillation source to the lung.

7.2 Future work

The aim of this thesis was to establish a better understanding of the transmission of pressure oscillations through the neonatal tracheobronchial tree. During this study a number of problems were identified which requires further future work to solve the problems.

- Casting process: while working with premature lamb lungs, it was not easy to get the exact measurement in terms of angle and thickness of the airway tree. This can be improved by applying a different method of painting the negative cast.
- Equipment: Having the right equipment is vital to get a better result. In order to detect the pressure oscillations at the level of secondary bronchi, a pressure sensor with a good position sensitivity than the current $\pm 5\text{mV}$ with smaller port diameter for thin branches will give a better result.
- Modelling: A model with compliant airways will be an improvement to better match the experimental result.

REFERENCES

1. Polin, R.A., et al. , *Fetal and Neonatal Physiology*. 2nd ed. Vol. 2. 1998: Pennsylvania: W.B Saunders Company.
2. Verder, H., et al., *Nasal continuous positive airway pressure and early surfactant therapy for respiratory distress syndrome in newborns of less than 30 weeks gestation*. *Pediatrics*, 1999. **103**.
3. Pillow, J., et al., *Bubble Continuous Positive Airway Pressure Enhances Lung Volume and Gas Exchange in Preterm Lambs*. *Am J Respir Crit Care Med*, 2007. **176**: p. 63-69.
4. Avery, M.E., et al. , *Is chronic lung disease in low birth weight infants preventable?* *Pediatrics*, 1987. **79**: p. 26-29.
5. DeKlerk, A.M. and R.K. DeKlerk, *Nasal continuous positive airway pressure and outcomes of preterm infants*. *Journal of Pediatric Child Health*, 1987. **79**: p. 26-29.
6. Claure, N., et al., *New modes of mechanical ventilation in the preterm newborn: evidence of benefit*. *ADC Fetal Neonatal Ed.*, 2007. **92**(6).
7. Ramanathan, R., *Synchronized Intermittent Mandatory Ventilation and Pressure Support: To Sync or Not to Sync? Pressure Support or No Pressure Support?* *Journal of Perinatology* 2005. **25**.
8. Mutch WA, et al., *Biologically variable ventilation prevents deterioration of gas exchange during prolonged anaesthesia*. *British journal of Anaesthesia*, 2000. **84**(2): p. 6.
9. McMullen, M., et al., *Biologically Variable Ventilation Improves Oxygenation and Respiratory Mechanics during One-lung Ventilation*. *Anesthesiology*, 2006. **105**(1): p. 91-97.
10. Sittig, S.E., *Neonatal Mechanical Ventilation Support*. AARC Time, 1999.
11. Courtney, S.E., et al., *High-Frequency Oscillatory Ventilation versus Conventional Mechanical Ventilation for Very-Low -Birth-Weight Infants*. *Pediatrics & Neonatology*, 2002. **347**: p. 10.
12. Rimensberger, P.C., et al., *First Intention High-Frequency Oscillation With Early Lung Volume Optimization Improves Pulmonary Outcome in Very Low Birth Weight Infants With Respiratory Distress Syndrome*. *Pediatrics & Neonatology*, 2000. **105**: p. 7.
13. Gittermann, M.K., et al., *Early nasal continuous positive airway pressure treatment reduces the need for intubation in very low birthweight infants*. *Eur J Pediatr*, 1997. **156**: p. 5.
14. Locke R, et al., *Effect of Nasal CPAP on thoracoabdominal motion in neonates with respiratory insufficiency*. *Pediatric* 1991. **11**(3): p. 6.
15. Graham M.R, et al., *Mathematical modelling to centre low tidal volumes following acute lung injury: A study with biologically variable ventilation*. *Respir Res.*, 2005 **28**(6): p. 64.
16. Mutch W. A., et al., *Biologically Variable or Naturally Noisy Mechanical Ventilation Recruits Atelectatic Lung*. *Am J Respir Crit Care Med* 2000. **162**: p. 4.
17. Arold, S.P., et al., *Variable Tidal Volume Ventilation Improves Lung Mechanics and Gas Exchange in a Rodent Model of Acute Lung Injury*. *Am J Respir Crit Care Med* 2002. **165**: p. 7.

18. Boker, A., et al., *Improved Arterial Oxygenation with Biologically Variable or Fractal Ventilation Using Low Tidal Volumes in a Porcine Model of Acute Respiratory Distress Syndrome* Am J Respir Crit Care Med, 2002. **165**: p. 7.
19. Fredberg, J.J., et al., *Mechanical Response of the Lungs at High Frequencies*. J Biomech Eng, 1978. **100**: p. 57- 65.
20. Fredberg, J.J., et al., *Canine Pulmonary Input Impedance Measured by Transient Forced Oscillations*. J Biomech Eng, 1978. **100**: p. 57-65.
21. Gil, J., *Models of lung disease: microscopy and structural methods* Vol. 47, New York: Academic Press. 12.
22. Horsfield K, *Methods for casting airways*. In: *Models of disease: Microscopy and structural methods* Dekker, 1990. **47**: p. 265-277.
23. Davies, A., *The evolution of bronchial casts*. Med. Hist, 1973. **17**: p. 386-391.
24. Dekker, E., *Transition between laminar and turbulent flow in human trachea*. J. Appl. Physiology, 1961. **1**: p. 1060-1064.
25. Timbrell, V., et al., *Hollow casts of lungs for experimental purposes*. Nature 1970. **225**: p. 97-98.
26. Tamai, S., et al., *Technique for making a Vascular Corrosion Mask*, in *Experimental and clinical reconstructive microsurgery*, T. Sempuku, Editor. 2003, Springer. p. 57.
27. Liebow, A.A., et al., *Plastic demonstrations of pulmonary pathology*. Bull Int Ass Med Museums, 1947. **27**: p. 116-129.
28. Tompsett, D.H., *A new method for preparation of bronchopulmonary casts*. Thorax, 1952. **7**: p. 78-88.
29. West, J.B., et al. , *Patterns of gas flow in the upper bronchial tree*. J. Appl. Physiology, 1959. **14**: p. 753-759.
30. Phalen, R.F., et al., *Casting the lungs in situ*. Anatomical Record, 1973. **177**: p. 255-263.
31. Raabe, O.G., et al., *Tracheobronchial Geometry: Human, Dog, Rat, Hamster*. Lovelace Found. Medical Ed. Res, 1976.
32. Schreider, J.P. and G. Raabe, *Replica casts of the entire respiratory airways of experimental animals*. J. Environ. Pathol.Toxicol, 1980. **3**: p. 427-435.
33. Frank, N.R. and R.E. Yoder, *A method of making a flexible cast of the lung*. J. Appl. Physiol., 1966 **21**: p. 1925-1926.
34. Viggiano, D., et al., *A New Method to Make Vascular and Bronchial Casts of Voluminous Organs*. European Journal of Morphology, 2003. **41**(5): p. 161-165.
35. Perry, S.F., et al., *Bronchial casts of human lungs using negative pressure injection*. Experimental Lung Research, 2000. **26**: p. 27-39.
36. Pedersen, C.J., et al *Technique for making hollow central airway casts*. California Primate Research Center, 1983. **55**(1): p. 254-257.
37. Wikipedia, *Latex*. 2011.
38. Eisman, M.M., *Lung models: hollow, flexible reproductions*. Journal of Applied Physiology, 1970. **29**.
39. Wikipedia, *Silicone rubber*. 2011.
40. Snyder, B. and M.J. Jaeger, *Lobar flow patterns in a hollow cast of canine central airways*. 1983. **54**(3): p. 749-756.
41. Schlesinger, R.B., et al., *Particle deposition in a hollow cast of the Human Tracheobronchial Tree*. Pergamon Press, 1977. **8**: p. 429-445.
42. Reddy, P., *The Effect of Pressure Oscillation on Respiratory Performance*, PHD Thesis, in *Institute of Biomedical Technologies*. 2009, AUT University: Auckland.

43. Gauthier, S.P., et al., *Structure-Function of Airway Generation 0 to 4 in the Preterm Lamb*. *Pediatric*, 1992. **31**(2).
44. Reddy, P., *The Effect of Pressure Oscillations on Neonatal Breathing*, *Master of Engineering Thesis*, in *Diagnostics and Control Research Centre*. 2004, Auckland University of Technology: Auckland.
45. Pillow, J., et al., *Effects of Gestation and Antenatal Steroid on Airway and Tissue Mechanics in Newborn Lambs*. *Am. J. Respir. Crit. Care Med.*, 2001. **163**(5): p. 1158-1163.
46. Willet, K.E., et al., *Pulmonary Interstitial Emphysema 24 Hours after Antenatal Betamethasone Treatment in Preterm Sheep*. *Am. J. Respir. Crit. Care Med.*, 2000. **162**(3): p. 1087-1094.
47. Reynolds, D.B. and J.S. Lee, *Steady pressure-flow relationship of a model of the canine bronchial tree*. *Journal of Applied Physiology*, 1981. **51**(5): p. 1072-1079.
48. Kilpper, R.W. and P.J. Stidd, *A wet lung technique for obtaining silastic rubber casts of the respiratory airways*. *Anat. Rec.*, 1973. **176**: p. 279-288.
49. Peterson, A.K., *On the preparation of Woods metal casts of the lungs*. *Anat. Rec.*, 1935. **61**: p. 261-272.
50. Reddy, P.I. and A.M. Al-Jumaily, *Understanding the use of continuous oscillating positive airway pressure (bubble CPAP) to treat neonatal respiratory disease: An engineering approach*. *Journal of Medical Engineering & Technology* 2009. **33**(3): p. 214-222.
51. Schmidt, M., et al., *Computer simulation of the measured respiratory impedance in newborn infants and the effect of the measurement equipment*. *Medical Engineering & Physics*, 1998. **20**: p. 220 – 228.

APPENDICES

APPENDIX A: Matlab program

```
for j=1:5
Fs = 1000;           % Sampling frequency

x= Sheet1(:,j);

L = length (x);     % 58180 Length of signal

NFFT = 2^nextpow2(L); % Next power of 2 from length of data.
                    % this function is useful for
                    %optimizing FFT operations, which are
                    %most efficient when sequence length is
                    %an power of two.

%NFFT=65536

Y = fft(x,NFFT)/L;

R=2*abs(Y(1:NFFT/2+1)); % Get absolute value of Y, from 1 up
                       %to NFFT/2+1

f = Fs/2*linspace(0,1,NFFT/2+1); %generates a row vector f
                                   %with NFFT/2+1 much points
                                   %linearly spaced Starting
                                   %from 0 and FS/2.

MXstore(:,j)=R;

end

a=find(f>10,1); % returns a one position where f is greater
               %than 10.

Zdata(2,1)= mean (MXstore((a-5:a+5),3)./MXstore((a-
5:a+5),2));
hold on
Zdata(2,2)= mean(MXstore((a-5:a+5),4)./MXstore((a-5:a+5),2));
hold on
Zdata(2,3)= mean(MXstore((a-5:a+5),5)./MXstore((a-5:a+5),2));

plot(Zdata')
```

Appendix B: Flow Chart

